Published in final edited form as:

Inorg Chem. 2006 April 17; 45(8): 3424–3436. doi:10.1021/ic0520465.

Synthetic Analogues of the Active Site of the A-cluster of Acetyl Coenzyme A Synthase/CO Dehydrogenase: Syntheses, Structures, and Reactions with CO

Todd C. Harrop[a], **Marilyn M. Olmstead**[b], and **Pradip K. Mascharak**[*,a]

[a]Department of Chemistry and Biochemistry, University of California, Santa Cruz, CA 95064

[b]Department of Chemistry, University of California, Davis, CA 95616

Abstract

Two metallosynthons, namely $(Et_4N)_2$[Ni(NpPepS)] (**1**) and $(Et_4N)_2$[Ni(PhPepS)] (**2**) containing carboxamido-N and thiolato-S as donors have been used to model the bimetallic M_p-Ni_d subsite of the A-cluster of the enzyme ACS/CODH. A series of sulfurbridged Ni/Cu dinuclear and trinuclear complexes (**3**-**10**) have been synthesized to explore their redox properties and affinity of the metal centers toward CO. The structures of $(Et_4N)_2$[Ni(PhPepS)] (**2**), (Et_4N)[Cu(neo)Ni(NpPepS)]•0.5Et_2O•0.5H_2O (**3**•0.5Et_2O•0.5H_2O), (Et_4N)[Cu(neo)Ni(PhPepS)]•H_2O (**4**•H_2O), $(Et_4N)_2$[Ni{Ni(NpPepS)}$_2$]•DMF (**5**•DMF), $(Et_4N)_2$[Ni(DMF)$_2${Ni(NpPepS)}$_2$]•3DMF (**6**•3DMF), $(Et_4N)_2$[Ni(DMF)$_2${Ni(PhPepS)}$_2$] (**8**), and [Ni(dppe)Ni(PhPepS)]•CH_2Cl_2 (**10**•CH_2Cl_2) have been determined by crystallography. The Ni_d mimics **1** and **2** resist reduction and exhibit no affinity toward CO. In contrast, the sulfur-bridged Ni center (designated Ni_C) in the trinuclear models **5**–**8** are amenable to reduction and binds CO in the Ni(I) state. Also, the sulfur-bridged Ni_C center can be removed from the trimers (**5**–**8**) by treatment with 1,10-phenanthroline much like the “labile Ni” from the enzyme. The dinuclear Ni-Ni models **9** and **10** resemble the Ni_p-Ni_d subsite of the A-cluster more closely and only the modeled Ni_p site of the dimers can be reduced. The Ni(I)-Ni(II) species display EPR spectra typical of a Ni(I) center in distorted trigonal bipyramidal and distorted tetrahedral geometries for $\mathbf{9_{red}}$ and $\mathbf{10_{red}}$, respectively. Both species bind CO and the CO-adducts $\mathbf{9_{red}}$**-CO** and $\mathbf{10_{red}}$**-CO** display strong ν_{CO} at 2044 and 1997 cm^{-1}, respectively. The reduction of **10** is reversible. The CO-affinity of **10** in the reduced state and the ν_{CO} value of $\mathbf{10_{red}}$**-CO** closely resemble the CO-bound reduced A-cluster (ν_{CO} = 1996 cm^{-1}).

[*]pradip@chemistry.ucsc.edu (P. K. Mascharak), Fax: + 1-831-459-2935 Tel: + 1-831-459-4251.

Supporting Information Available: The FTIR spectra of **10** and $\mathbf{10_{red}}$**-CO** in KBr matrix (Figure S1), machine parameters, crystal data, and data collection parameters for all the complexes (Table S1), selected bond distances and angles are reported (Table S2), and X-ray crystallographic data (in CIF format) and tables for the structure determination of complexes $(Et_4N)_2$[Ni(PhPepS)] (**2**), (Et_4N)[Cu(neo)Ni(NpPepS)]•0.5Et_2O•0.5H_2O (**3**•0.5Et_2O•0.5H_2O), (Et_4N)[Cu(neo)Ni(PhPepS)]•H_2O (**4**•H_2O), $(Et_4N)_2$[Ni{Ni(NpPepS)}$_2$]•DMF (**5**•DMF), $(Et_4N)_2$[Ni(DMF)$_2${Ni(NpPepS)}$_2$]•3DMF (**6**•3DMF), $(Et_4N)_2$[Ni(DMF)$_2${Ni(PhPepS)}$_2$] (**8**), and [Ni(dppe)Ni(PhPepS)]•CH_2Cl_2 (**10**•CH_2Cl_2). This material is available free of charge via the Internet at http://pubs.acs.org.

Introduction

Acetyl coenzyme A synthase/carbon monoxide dehydrogenase (ACS/CODH) is a bifunctional metalloenzyme that catalyzes two important biological reactions, namely the reversible reduction of CO_2 into CO (CODH activity) and the synthesis of acetyl coenzyme A (acetyl CoA) from CO, CH_3 from a methylated corrinoid iron-sulfur protein, and the thiol CoA (ACS activity).[1,2] Once formed, acetyl CoA is converted into cell carbon or respired as acetate depending on the metabolic needs of the cell. This enzyme is present in a number of anaerobic bacteria including acetogens, methanogens, and sulfate-reducers that utilize the Wood-Ljungdahl pathway for autotrophic carbon fixation.[3] Indeed, ACS/CODH has been implicated in the chemoautotrophic origin of life in which primitive organisms consumed CO or CO_2 from volcanic or hydrothermal sites for the formation of carbon-carbon bonds.[4] Interest in ACS/CODH stems from its unusual metallocluster active sites, role in the global carbon cycle (reducing the levels of gaseous pollutants like CO_2), and the reactions it catalyzes utilizing well known organometallic ligands like CO and CH_3, analogous to the industrial Monsanto acetic acid process.

Although a large volume of spectroscopic and biochemical data were available for the enzyme for some time,[1,2] the site of acetyl CoA synthesis (A-cluster) has come under intense scrutiny following the publication of three high-resolution crystal structures.[5-7] The A-cluster of ACS/CODH has been shown to exist in two different oxidation states, A_{ox} (S = 0) and A_{red}-CO (S = ½), the one electron reduced CO-adduct formed under CO atmosphere. The paramagnetic A_{red}-CO state is readily identified by a strong rhombic EPR signal (g = 2.08, 2.07, and 2.03) that exhibits dipolar broadening when isotopically substituted with ^{61}Ni, ^{57}Fe, or ^{13}CO (hence referred to as the NiFeC signal).[1,8] In addition, A_{red}-CO displays a strong band in its IR spectrum at 1996 cm^{-1} (ν_{CO}) consistent with a terminally bound CO molecule.[9] Addition of CH_3^+ to CO-treated ACS/CODH affords a diamagnetic state, although the order of CO and CH_3^+ binding is still debatable.[10] Titration of ACS/CODH with the bidentate chelator 1,10-phenanthroline (phen) results in the removal of ~ 30 % of the Ni present in the enzyme.[11] Such removal of “labile Ni” abolishes the NiFeC signal and also shuts down acetyl CoA synthesis with no effect on CODH activity. Reconstitution of phen-treated enzyme with $NiCl_2$ replenishes both the NiFeC signal and synthase activity.[11] These results strongly suggest that “labile Ni” is a requirement for ACS activity.

Crystallographic studies on ACS/CODH from the acetogenic bacterium *Moorella thermoacetica* (formerly known as *Clostridium thermoaceticum*) have revealed some interesting and unexpected features never seen before in any metalloenzyme. The overall $\alpha_2\beta_2$ protein comprises several metalloclusters in the different subunits.[5,6] The β subunits at the center of the protein contain the B, C, and D clusters, the site of CODH activity (C-cluster). The α-subunits, located at the terminal ends of the protein, contain the A-cluster, the site responsible for acetyl CoA formation. Interestingly, the structure of the A-cluster reported by two separate groups turned out to be quite different even though the enzyme was isolated from the same organism (*M. thermoacetica*). The first structure of ACS/CODH reported by Drennan and coworkers revealed a homodimeric $\alpha_2\beta_2$ protein whose active site is relatively unexposed to solvent that contain a trio of different metals present at the A-

cluster.[5] The A-cluster in the Drennan structure consists of an Fe_4S_4 cubane bridged through one Cys-S residue to a bimetallic site that contains a square-planar Ni(II) (Ni_d, distal to Fe_4S_4) ion with N_2S_2 coordination derived from two backbone carboxamido nitrogens and two Cys-S residues. The Ni_d site is further bridged through two Cys-S donors to a tetrahedral Cu(I) (M_p, proximal to Fe_4S_4) center. A fourth nonprotein ligand is also bound to Cu(I) to complete the coordination sphere (Figure 1). The second structure by Fontecilla-Camps and coworkers, however, revealed a very different A-cluster site.[6] First, the $\alpha_2\beta_2$ quaternary structure is no longer symmetric and consists of an $\alpha_c\beta\beta\alpha_o$ structure in which one of the α-subunits (α_o) is more open and exposed to solvent. In the A_o-cluster of α_o, a square-planar Ni(II) ion occupies the M_p site that is ~ 20 Å removed from a closed CO tunnel. Quite in contrast, the other α subunit (α_c) is closed off to solvent and a tetrahedral Zn(II) ion resides at the M_p site (Figure 1). This A_c-cluster is located at the end of an open hydrophobic CO tunnel from the C-cluster. The discrepancy in the structures of the A-cluster from the same enzyme triggered an intense debate regarding the identity of the true catalytic metal ion at the M_p site. The debate has recently subsided after careful biochemical[11a,12,13] and computational studies.[14,15] It is now evident that Ni at the M_p site is required for the ACS activity. A very recent structural study on an ACS/CODH from the hydrogenogenic bacterium *Carboxydothermus hydrogenoformans* has also revealed the presence of Ni at the M_p site.[7]

The extent to which the unusual coordination architecture of the A-cluster dictates its ability to assemble acetyl CoA is still an unanswered question. The presence of carboxamido-N donors at the Ni_d site is quite uncommon in biology. At this time, coordination of deprotonated carboxamido-N has only been observed in the oxidized P-cluster of nitrogenase[16], nitrile hydratase[17] (which contains a similar Cys-X-Cys metal binding motif as the Ni_d site), and most recently in Ni-SOD.[18] Since the publication of the first structure of ACS/CODH, several low molecular weight models of the ACS site have been synthesized and studied to determine the intrinsic properties of the metal-containing active site(s).[19-25] In these pursuits, researchers have focused mostly on the bimetallic M_p—Ni_d site of ACS and ignored the Fe_4S_4 portion (unlikely site of substrate binding). For example, Rauchfuss and coworkers have synthesized the model complex $[\{Ni(CO)_2\}\{NiS_2N'_2\}]^{2-}$ (structure a, Figure 2) with two terminal CO ligands bound to the bridged Ni center in the 0 oxidation state.[24] This complex was the first example of a structurally characterized, mixed-valence, sulfur-bridged, dinuclear Ni model containing carboxamido-N coordination that resembles the CO-bound form of the enzyme. More recently, Riordan and coworkers have employed the metallopeptide unit $[Ni(CGC)]^{2-}$ to synthesize biologically relevant Ni-Ni models like [Ni(CGC)Ni(dRpe)] (structure b, Figure 2).[20a] Although phosphine donors are not present in the enzyme, they do allow for more favorable reduction of the Ni_p site of the model to the Ni(I) state and binding of CO (as shown by electrochemistry). However, none of the models from this study has been characterized further by structural and spectroscopic (such as EPR, FTIR) studies. Clearly, more model complexes are required to establish the properties of the active site(s) of the ACS A-cluster and what implications these have on the overall mechanism of acetyl CoA synthesis.

As part of our continuing efforts on modeling the bimetallic M_p—Ni_d portion of the A-cluster of ACS, we describe herein the syntheses and properties of several di/trinuclear metal

complexes utilizing the dicarboxamido-dithiolato Ni(II) metallosynthons $(Et_4N)_2$[Ni(NpPepS)] (**1**)[26] and $(Et_4N)_2$[Ni(PhPepS)] (**2**) reported by us in preliminary accounts.[27] The redox behavior of two Cu(I)-Ni(II) models, namely (Et_4N)[Cu(neo)Ni(NpPepS)] (**3**) and (Et_4N)[Cu(neo)Ni(PhPepS)] (**4**) clearly demonstrate that catalytically active A-cluster cannot utilize Cu(I) at the M_p site. The four trinuclear models $(Et_4N)_2$[Ni{Ni(NpPepS)}$_2$] (**5**),[27b] $(Et_4N)_2$[Ni(DMF)$_2${Ni(NpPepS)}$_2$] (**6**),[27b] $(Et_4N)_2$[Ni{Ni(PhPepS)}$_2$] (**7**), and $(Et_4N)_2$[Ni(DMF)$_2${Ni(PhPepS)}$_2$] (**8**) and the two dinuclear models [Ni(terpy)Ni(NpPepS)] (**9**)[27a] and [Ni(dppe)Ni(PhPepS)] (**10**)[27a] provide the opportunity to study, for the first time, a series of complexes with variable donor sets and coordination geometries at the bridged Ni(II) center (Ni_p mimics). In this paper, we report the results of redox studies and CO binding at the M_p (M = Cu, Ni) centers of these models and compare the spectral data of the reduced CO-adducts with that of the A_{red}-CO ($S = ½$) signal of the enzyme in order to establish the mode of CO binding by the A-cluster of ACS/CODH.

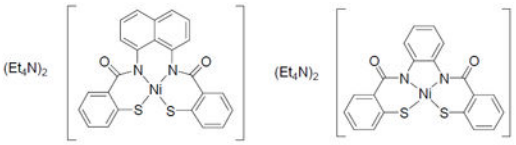

(**1**) (**2**)

Experimental Section

Thiosalicylic acid, 1,2-phenylenediamine, 1,8-diaminonaphthalene, triethylamine, [Ni(dppe)Cl_2], CuCl, [Cu(MeCN)$_4$]PF_6, 2,9-dimethyl-1,10-phenanthroline (neocuproine, abbreviated as neo), 2,2′:6′,2″-terpyridine (terpy), 1,2-ethanedithiol (edt), and 1,10-phenanthroline (phen) were purchased from Aldrich Chemical Co. and used without further purification. $NpPepSH_4$ (*N,N*′-naphthalenebis(*o*-mercaptobenzamide)[26], 2,2'-dithiosalicyl chloride[26], $(Et_4N)_2$[Ni(NpPepS)][26] (**1**), $(Et_4N)_2$[$NiCl_4$][28], [Cu(neo)Cl][29a], $(Na)_3$[Cu_3(edt)$_3$][29b], and [Ni(terpy)Cl_2][30] were synthesized by following published procedures. All manipulations were carried out under N_2 (where needed) using Schlenk lines or dry box techniques. The solvents were purified by standard techniques and distilled prior to use.

Synthesis of Compounds. $PhPepSH_4$ (*N,N*′-phenylenebis(*o*-mercaptobenzamide)

The synthesis of the ligand comprises the following steps.

Step 1. $(PhPepS-)_2$

A solution of 1,2-phenylenediamine (0.23 g, 2.13 mmol) and triethylamine (0.67 g, 6.63 mmol) dissolved in 10 mL of CH_2Cl_2 was quickly added to a solution of 2,2'-dithiosalicyl chloride (0.72 g, 2.10 mmol) in 10 mL CH_2Cl_2. The resulting pale yellow-brown solution was stirred for 48 h at room temperature. This solution was then washed with aqueous $NaHCO_3$ and NaCl. The CH_2Cl_2 layer was dried with $MgSO_4$, filtered, and the solvent was removed by rotary evaporation to yield an oily yellow residue. The oil was triturated three times with Et_2O (10 mL) to afford a pale yellow solid. Yield: 0.32 g (41 %). ^{1}H NMR (298

K, $CDCl_3$, 500 MHz): δ (ppm from TMS) 8.59 (s, 1H, NH), 7.67 (d, 1H), 7.53 (t, 1H), 7.39 (m, 2H), 7.21 (m, 2H). Selected IR bands (KBr matrix, cm^{-1}): 3217 (m, ν_{NH}), 1652 (vs, ν_{co}).

Step 2. $PhPepSH_4$

To a degassed THF solution (10 mL) of (PhPepS-)$_2$ (0.32 g, 0.85 mmol) was slowly added solid $NaBH_4$ (0.17 g, 4.49 mmol) in small portions at 4 °C. The bright yellow-orange solution was then allowed to stir at room temperature for 16 h. Next, the THF solution was concentrated to ~10 % of the original volume via short-path vacuum distillation and 6 M acetic acid was added dropwise at 4 °C until the pH was 3. The light cream colored solid that precipitated almost immediately upon addition of acid was collected by filtration, washed with degassed water, and dried on a high-vacuum line for 2 h. Yield: 0.30 g (90 %). ^{1}H NMR (298 K, $CDCl_3$, 500 MHz): δ (ppm from TMS) 8.73 (s, 1H, NH), 7.69 (d, 1H), 7.56 (t, 1H), 7.36 (d, 1H), 7.31 (t, 1H), 7.22 (m, 2H), 4.53 (br s, 1H, SH). Selected IR bands (KBr plates, cm^{-1}): 3300 (m, ν_{NH}), 2552 (w, ν_{SH}), 1652 (vs, ν_{co}).

$(Et_4N)_2$[Ni(PhPepS)] (2)

A batch of NaH (0.054 g, 2.24 mmol) was added to a solution of $PhPepSH_4$ (0.17 g, 0.45 mmol) in 10 mL of degassed DMF and the pale yellow-brown solution was allowed to mix for ~ 20 min to ensure that all NaH had reacted. To this solution was then added a batch of $(Et_4N)_2[NiCl_4]$ (0.21 g, 0.44 mmol) dissolved in 2 mL of DMF. The dark red-brown solution thus obtained was stirred for 4 h at room temperature. Next, DMF was removed via short-path vacuum distillation and the residue was dissolved in 25 mL of MeCN and filtered. The resulting red solution was concentrated to ~ 50 % of the original volume and the desired product was isolated as a red microcrystalline solid. Yield: 0.25 g (82 %). Anal calcd. for $C_{36}H_{52}N_4O_2S_2Ni$ (**2**): C, 62.16; H, 7.53; N, 8.05; found: 62.11; H, 7.61; N, 8.02. Selected IR bands (KBr plates, cm^{-1}): 1521 (vs, ν_{co}). Electronic absorption spectrum in MeCN, λ_{max} nm (ε, M^{-1} cm^{-1}): 545 (sh 610), 384 (8 845), 331 (19 510). ^{1}H NMR (298 K, CD_3CN, 500 MHz): δ (ppm from TMS) 8.06 (d, 1H), 7.95 (d, 1H), 7.22 (d, 1H), 6.78 (m, 2H), 6.51 (t, 1H), 3.14 (q, 8H), 1.11 (t, 12H).

(Et_4N)[Cu(neo)Ni(NpPepS)] (3)

A batch of 0.04 g (0.14 mmol) of [Cu(neo)Cl] was added to a red-orange solution of 0.10 g (0.14 mmol) of **1** in 10 mL of DMF. The burgundy red homogeneous solution thus obtained was stirred for 12 h at room temperature. Next, DMF was removed in vacuo and 10 mL of MeCN was added to the residue. The pale red solution with a dark precipitate was filtered and the dark red solid was washed with 10 mL of MeCN and dried in vacuo. Yield: 0.087 g (71 %). Anal calcd. for $C_{46}H_{46}N_5O_2S_2CuNi$ (**3**): C, 62.27; H, 5.23; N, 7.89; found: 62.14; H, 5.31; N, 7.92. Selected IR bands (KBr plates, cm^{-1}): 1516 (vs, ν_{co}). Absorption spectrum in MeCN, λ_{max} nm (ε, M^{-1} cm^{-1}): 495 (12 250), 420 (12 130), 326 (32 000). ^{1}H NMR (298 K, CD_3CN, 500 MHz): δ (ppm from TMS) 8.43 (d, 1H), 7.96 (s, 1H), 7.93 (d, 1H), 7.68 (d, 1H), 7.50 (t, 2H), 7.17 (t, 1H), 6.93 (t, 1H), 6.50 (d, 1H), 6.43 (t, 1H), 3.11 (q, 4H), 2.74 (s, 3H), 1.16 (t, 6H).

$(Et_4N)[Cu(neo)Ni(PhPepS)]$ (4)

A batch of 0.05 g (0.16 mmol) of [Cu(neo)Cl] was slowly added to a solution of 0.11 g (0.15 mmol) of **2** in 15 mL of MeCN. The deep burgundy red solution was then stirred at room temperature for 2 h. Next, the solvent was removed via short path vacuum distillation and the red oily residue was triturated with 20 mL of degassed MeCN/Et_2O (1:1) mixture. The red solid thus obtained was collected by filtration, washed with cold Et_2O, and dried on a high-vacuum line for 1 h. Yield: 0.086 g (66 %). Anal calcd. for $C_{42}H_{44}N_5O_2S_2CuNi$ (**4**): C, 60.25; H, 5.30; N, 8.37; found: 60.34; H, 5.23; N, 8.39. Selected IR bands (KBr plates, cm^{-1}): 1524 (vs, ν_{co}). Absorption spectrum in MeCN, λ_{max} nm (ε, M^{-1} cm^{-1}): 495 (2 940), 363 sh (10 650), 312 sh (19 600). ^1H NMR (298 K, CD_3CN, 500 MHz): δ (ppm from TMS) 8.40 (d, 1H), 8.11 (s, 1H), 7.94 (d, 1H), 7.84 (d, 1H), 7.67 (t, 1H), 6.75 (t, 1H), 6.62 (t, 1H), 6.50 (d, 1H), 6.31 (t, 1H), 3.34 (s, 3H), 3.12 (q, 4H), 1.17 (t, 6H).

$(Et_4N)_2[Ni\{Ni(NpPepS)\}_2]$ (5)

A batch of 0.027 g of $(Et_4N)_2[NiCl_4]$ (0.059 mmol) dissolved in 2 mL MeCN was added to a solution containing 0.087 g (0.117 mmol) of **1** in 10 mL of degassed MeCN. The initial red-orange color of the solution turned pale orange and a dark red microcrystalline precipitate appeared within minutes. This heterogeneous solution was stirred for 1 h and then the mixture was filtered. The microcrystalline dark solid was collected, washed with dry Et_2O, and dried in vacuo. Yield: 0.065 g (85 %). Anal calcd. for $C_{64}H_{68}N_6O_4S_4Ni_3$ (**5**): C, 59.61; H, 5.31; N, 6.52; found: 59.70; H, 5.27; N, 6.51. Selected IR bands (KBr plates, cm^{-1}): 1538 (vs, ν_{co}).

$(Et_4N)_2[Ni(DMF)_2\{Ni(NpPepS)\}_2]$ (6)

A batch of 0.053 g (0.04 mmol) of **5** was allowed to stir for 2 h at room temperature in 10 mL of degassed DMF. The initial heterogeneous solution slowly became homogeneous and turned bright red in color. The DMF was removed via vacuum distillation and the resulting oily red material was triturated with 10 mL of dry Et_2O to obtain the desired product as a fine red solid. Yield: 0.053 g (94 %). Anal calcd. for $C_{70}H_{82}N_8O_6S_4Ni_3$ (**6**): C, 58.56; H, 5.76; N, 7.80; found: 58.64; H, 5.73; N, 7.79. Selected IR bands (KBr plates, cm^{-1}): 1645 (s, ν_{co} DMF), 1532 (vs, ν_{co}). Absorption spectrum in DMF, λ_{max} nm (ε, M^{-1} cm^{-1}): 525 (sh), 437 (12 410).

$(Et_4N)_2[Ni\{Ni(PhPepS)\}_2]$ (7)

A solution of 0.035 g of $(Et_4N)_2[NiCl_4]$ (0.075 mmol) dissolved in 3 mL of MeCN was added to a red-orange solution of 0.102 g (0.147 mmol) of **2** in 20 mL of degassed MeCN. The color of the reaction mixture rapidly turned to dark red. The deep red solution was stirred for 1 h at room temperature and then its volume was reduced to half by short path vacuum distillation. Storage of this solution at −20 °C for 16 h resulted in the precipitation of a red crystalline solid. This microcrystalline red solid was collected, washed with dry Et_2O, and dried in vacuo. Yield: 0.080 g (92 %). Anal calcd. for $C_{56}H_{64}N_6O_4S_4Ni_3$ (**7**): C, 56.55; H, 5.42; N, 7.07; found: 56.64; H, 5.37; N, 7.10. Selected IR bands (KBr plates, cm^{-1}): 3052 (w), 2983 (w), 1591 (s), 1566 (s), 1538 (vs, ν_{co}), 1467 (s), 1442 (s), 1393 (w), 1345 (s), 1295 (w), 1268 (m), 1220 (w), 1182 (w), 1172 (w), 1140 (w), 1118 (w), 1059 (w),

1040 (w), 1002 (w), 956 (w), 791 (w), 755 (m), 691 (w), 601 (w), 515 (w). Absorption spectrum in MeCN, λ_{max} nm (ε, M^{-1} cm^{-1}): 850 sh (800), 660 (2500), 560 sh (3030), 470 (3850). ^{1}H NMR (298 K, CD_3CN, 500 MHz): δ (ppm from TMS) 8.07 (d, 1H), 7.95 (d, 1H), 7.21 (d, 1H), 6.78. (m, 2H), 6.50 (t, 1H), 3.14 (q, 4H), 1.13 (t, 6H).

$(Et_4N)_2[Ni(DMF)_2\{Ni(PhPepS)\}_2]$ (8)

A batch of 0.027 g (0.022 mmol) of **7** was allowed to stir for 2 h at room temperature in 5 mL of degassed DMF. Next, the solvent was removed via vacuum distillation and the resulting oily red material was triturated with 5 mL of dry Et_2O to obtain the desired product as a fine red solid. Yield: 0.028 g (97 %). Anal calcd. for $C_{62}H_{78}N_8O_6S_4Ni_3$ (**8**): C, 55.75; H, 5.89; N, 8.39; found: 55.74; H, 5.83; N, 8.41. Selected IR bands (KBr plates, cm^{-1}): 1646 (vs, ν_{co} DMF), 1538 (vs, ν_{co}). Absorption spectrum in DMF, λ_{max} nm (ε, M^{-1} cm^{-1}): 527 (1080), 380 sh (15 300), 335 (38 130).

[Ni(terpy)Ni(NpPepS)] (9)

A slurry of 0.048 g (0.13 mmol) of [Ni(terpy)Cl_2] in 1 mL of MeCN was added to a solution containing 0.100 g (0.13 mmol) of **1** in 10 mL MeCN. Within 5 min, the initial red-orange solution turned pale and a red-brown precipitate appeared. The precipitate was filtered, washed with cold MeCN, and dried in vacuo. Yield: 0.076 g (75 %). Anal calcd. for $C_{39}H_{25}N_5O_2S_2Ni_2$ (**9**): C, 60.27; H, 3.24; N, 9.01; found: 60.21; H, 3.30; N, 8.97. Selected IR bands (KBr plates, cm^{-1}): 3051 (w), 1585 (s), 1568 (s), 1531 (vs, ν_{co}), 1474 (m), 1451 (m), 1429 (w), 1385 (s), 1355 (m), 1321 (w), 1265 (w), 1248 (w), 1184 (w), 1163 (w), 1112 (w), 1095 (w), 1054 (w), 1035 (w), 1016 (w), 958 (w), 820 (w), 771 (m), 742 (m), 680 (w), 650 (w), 642 (w), 619 (w), 592 (w). Absorption spectrum in DMF, λ_{max} nm (ε, M^{-1} cm^{-1}): 450 sh (8500), 427 (10 200), 337 (34 680).

[Ni(dppe)Ni(PhPepS)] (10)

A batch of 0.154 g (0.292 mmol) of [Ni(dppe)Cl_2] was slowly added to a solution of 0.204 g (0.293 mmol) of **2** in 10 mL of MeCN. Almost immediately, the red-brown solution turned pale and a blue-green microcrystalline solid appeared in the reaction mixture. The solid was filtered, washed with cold MeCN, and dried in vacuo. Yield: 0.223 g (85 %). Anal calcd. for $C_{46}H_{46}N_5O_2S_2CuNi$ (**10**): C, 61.92; H, 4.07; N, 3.14; found: 62.03; H, 4.16; N, 3.12. Selected IR bands (KBr plates, cm^{-1}): 1538 (vs, ν_{co}). Electronic absorption spectrum in CH_2Cl_2, λ_{max} nm (ε, M^{-1} cm^{-1}): 594 (3 040), 506 (sh 1 890), 345 (21 910). ^{1}H NMR (298 K, $CDCl_3$, 500 MHz): δ (ppm from TMS) 8.03 (m, 2H), 7.90 (s, 2H), 7.61 (s, 5H), 7.39 (s, 1H), 7.31 (s, 2H), 6.96 (t, 1H), 6.74 (t, 1H), 6.51 (t, 1H), 6.43 (d, 1H), 1.87 (t, 2H).

Physical Measurements

Electronic absorption spectra were recorded on a Perkin-Elmer Lambda 9 UV/Vis/NIR Spectrophotometer. A Perkin-Elmer Spectrum One or Nicolet Nexus 870 FTIR was used to monitor the infrared spectra. The ^{1}H NMR spectra were recorded at 298 K on a Varian Unity Plus 500 MHz spectrometer. EPR spectra were collected on a Bruker EleXsys E500 spectrometer at X-band frequencies at liquid N_2 temperature. A Johnson-Matthey magnetic susceptibility balance was used to determine the room-temperature magnetic susceptibility

values of the solid complexes. Electrochemical measurements were performed with Princeton Applied Research instrumentation (model 273A) at 298 K in DMF or CH_2Cl_2 using either 0.1 M $(Et_4N)(ClO_4)$ or $(n-Bu_4N)(PF_6)$ as the supporting electrolyte. The working electrode was a Beckman Pt-inlay working electrode and the potentials were measured versus a saturated calomel electrode (SCE).

X-ray Data Collection and Structure Solution and Refinement

Red needles of $(Et_4N)_2$[Ni(PhPepS)] (**2**) were grown by slow diffusion of Et_2O into a dilute solution of **2** in MeCN at 4 °C. Red plates of (Et_4N)[Cu(neo)Ni(NpPepS)]•0.5Et_2O•0.5H_2O (**3**•0.5Et_2O•0.5H_2O) were obtained from slow diffusion of Et_2O into a saturated solution of **3** in MeCN/DMF (1/1). Red needles of (Et_4N)[Cu(neo)Ni(PhPepS)]•H_2O (**4**•H_2O) were obtained upon slow cooling of an MeCN/Et_2O (1/1) solution of the complex at −20 °C. Black blocks of $(Et_4N)_2$[Ni{Ni(NpPepS)}$_2$]•DMF (**5**•DMF) were obtained by slow diffusion of Et_2O into a saturated solution of the complex in MeCN/DMF (9/1). Red parallelepipeds of $(Et_4N)_2$[Ni(DMF)$_2${Ni(NpPepS)}$_2$]•3DMF (**6**•3DMF) were grown by diffusion of Et_2O into a dilute solution of the complex in DMF. Red blocks of $(Et_4N)_2$[Ni(DMF)$_2${Ni(PhPepS)}$_2$] (**8**) were grown by slow diffusion of Et_2O into a dilute solution of the complex in DMF. Black prisms of [Ni(dppe)Ni(PhPepS)]•CH_2Cl_2 (**10**•CH_2Cl_2) were obtained from slow evaporation of a concentrated solution of **10** in a CH_2Cl_2/toluene (3/1) mixture at room temperature. Diffraction data for **2, 4**•H_2O, and **10**•CH_2Cl_2 were collected at 91 K on a Bruker APEX system. Diffraction data for **3**•0.5Et_2O•0.5H_2O, **5**•DMF, and **8** were collected at 91 K on a Bruker SMART 1000 system. For these structures Mo Kα (0.71073 Å) radiation was used and the data were corrected for absorption. Diffraction data for **6**•3DMF were collected at 130 K on a Siemens P4 system. Cu Kα (1.54178 Å) radiation was used and the data were corrected for absorption. The structures were solved using the standard SHELXS-97 package. Machine parameters, crystal data, and data collection parameters for all the complexes are summarized in Table S1 while selected bond distances and angles are reported in Table S2. Both these tables have been submitted as Supporting Information along with other crystallographic data for all of the complexes.

Results and Discussion

Synthesis

The Ni_d mimics $(Et_4N)_2$[Ni(NpPepS)] (**1**)[26] and $(Et_4N)_2$[Ni(PhPepS)] (**2**)[27a] served as the metallosynthons in the construction of the higher nuclearity analogues reported in this account. To date, several Ni(II)-dicarboxamido-dithiolato complexes have been reported in the literature.[19,21,31-33] The synthetic route that we have followed to obtain the Ni(II) complexes **1** and **2** was originally developed in this laboratory for the synthesis of Fe(III)-carboxamide complexes.[34] Reaction of $(Et_4N)_2[NiCl_4]$ with the deprotonated (with the aid of NaH) ligands $NpPepS^{4-}$ or $PhPepS^{4-}$ in solvents like DMF readily afford complexes **1** and **2** in high yields. These Ni(II) complexes with N_2S_2 chromophores are inherently stable in the solid state.

Failures in the initial attempts to synthesize Ni-Cu dinuclear model complexes in the present work provide some synthetic tips for isolation of such systems. Addition of simple Cu(I) salts like CuCl or $[Cu(MeCN)_4]PF_6$ to DMF solutions of the Ni_d mimic **1** invariably results in the formation of the trinuclear species $(Et_4N)[Cu\{Ni(NpPepS)\}_2]$ regardless of the choice of solvent, Cu(I) salt, or reagent stoichiometry.[27b] This observation suggests that in order to synthesize discrete dinuclear species, one must employ Cu(I) starting complexes with less labile ligands. Use of the trinuclear Cu(I) complex, $[Cu_3(edt)_3]^{3-}$ (edt = 1,2-ethanedithiol)[29b], however, leads to no reaction with **1** or **2** in solvents like DMF, MeCN, or MeOH at room temperature. When reaction mixtures with **1** is heated to 65 °C in DMF for 24 h, one obtains the trinuclear complex $(Et_4N)[Cu\{Ni(NpPepS)\}_2]$ instead of the desired S-bridged Ni-Cu complex $[Cu(edt)Ni(NpPepS)]^{3-}$. In contrast, when one employs [Cu(neo)(Cl)][29a] (neo = neocuproine = 2,9-dimethyl-1,10-phenanthroline) as the starting Cu(I) complex, the reaction indeed takes the desired course. For instance, reaction of [Cu(neo)Cl] with **1** or **2** in MeCN at room temperature cleanly affords the Ni-Cu dinuclear complexes $(Et_4N)[Cu(neo)Ni(NpPepS)]$ (**3**) and $(Et_4N)[Cu(neo)Ni(PhPepS)]$ (**4**), respectively in high yields. Clearly, the strong preference of the neocuproine ligand for Cu(I) centers as well as the tetrahedral geometric preference of Cu(I) allows for the formation of **3** and **4**. Complexes **3** and **4** were also obtained when [Cu(neo)(SR)] (R = C_6H_5, p-C_6H_4-Cl)[29c] are used as the starting Cu(I) complexes. In the solid state, **3** and **4** are stable for months and no oxidation of the Cu(I) center is observed (as verified by ^{1}H NMR and electronic absorption spectroscopy).

Similar reactivity has also been noted in our attempts to synthesize dinuclear Ni(II) species. Reactions of Ni(II) salts like $(Et_4N)_2[NiCl_4]$ with **1** or **2** in MeCN afford the corresponding trinuclear complexes $(Et_4N)_2[Ni\{Ni(NpPepS)\}_2]$ (**5**) and $(Et_4N)_2[Ni\{Ni(PhPepS)\}_2]$ (**7**) in high yield. These trinuclear complexes form regardless of the Ni(II) salt/metallosynthon stoichiometry. Isolation of these complexes is aided by the high insolubility of **5** and **7** in MeCN; the trinuclear complexes precipitate out of solution within minutes. Interestingly, dissolution of **5** and **7** in DMF (a slow process) results in coordination of two molecules of DMF to the central Ni(II) ion (designated as Ni_C) affording the DMF adducts $(Et_4N)_2[Ni(DMF)_2\{Ni(NpPepS)\}_2]$ (**6**) and $(Et_4N)_2[Ni(DMF)_2\{Ni(PhPepS)\}_2]$ (**8**), respectively. This binding is also reversible. When the DMF adducts **6** and **8** are treated with solvents like MeCN or THF, the respective trinuclear species **5** and **7** form almost immediately (verified by IR and ^{1}H NMR).

The dinuclear Ni-Ni model complexes have been synthesized by following the strategy used to isolate the Ni-Cu complexes **3** and **4**. Reaction of one equiv of $[Ni(terpy)Cl_2]$ (terpy = 2,2′:6′,2″-terpyridine) with **1** in MeCN affords [Ni(terpy)Ni(NpPepS)] (**9**), a Ni-Ni dimer in which the modeled Ni_p site is five-coordinate. The isolation of **9** is aided by its lack of solubility in a variety of polar solvents like MeOH and MeCN due to the overall neutral charge of the complex. Since the as isolated Ni_p site of ACS is four-coordinate in the crystal structure, we employed a second Ni_p synthon, $[Ni(dppe)Cl_2]$ (dppe = 1,2-bis(diphenylphosphino)ethane), in such reaction. This Ni_p synthon is expected to favor an easier reduction to the Ni(I) oxidation state and further facilitate binding of CO. However, all attempts to synthesize a Ni-Ni dimer with **1** and $[Ni(dppe)Cl_2]$ led to the formation of the

trinuclear species **5**. In contrast, reaction of **2** with 1 equiv of [Ni(dppe)Cl_2] in MeCN affords [Ni(dppe)Ni(PhPepS)] (**10**) as a blue-green microcrystalline solid in 85 % yield. Steric interactions between the folded structure of the {Ni(NpPepS)} moiety[26] and the dppe ligand frame presumably prevent the formation of the dinuclear complex in the first case while the more rigid ligand frame of **2** allows formation of the desired dimer **10** without such hindrance. It is therefore evident that proper design of the ligand frame of the Ni_d metallosynthon is crucial for the successful isolation of Ni_p-Ni_d ACS models.

Structure and Properties. $(Et_4N)_2$[Ni(PhPepS)] (2)

The structure of $[Ni(PhPepS)]^{2-}$ (anion of **2**) is shown in Figure 3. The coordination geometry around nickel is square-planar arising from two carboxamido nitrogens and two thiolato sulfurs in *cis* geometry. Although the overall disposition of the $PhPepS^{4-}$ ligand frame is similar to that of $NpPepS^{4-}$ in $(Et_4N)_2$[Ni(NpPepS)] (**1**),[26] there are some noted differences. For example, the extent of the 'butterfly' folding of the aryl sulfur rings observed in **1** is not as extreme in the case of **2**. This is reflected in the more rigid fivemember chelate ring of the phenylenediamido portion of **2** (nearly coplanar with the NiN_2S_2 plane) compared to the six-member chelate ring of the naphthalenediamido portion of **1** (almost perpendicular to the NiN_2S_2 plane). Interestingly, [Ni(tsalphen)], an analogous Ni(II) complex derived from a ligand frame similar to **2** but with imine nitrogen coordination, is completely planar.[35] This suggests that the bending of the aryl rings are most likely due to the presence of the carboxamido nitrogens in **2**. The angles at the Ni(II) center are slightly distorted from the ideal 90° value due to the short bite of the phenylenediamido portion of the ligand frame (N1–Ni–N2, 85.52(11)°). The average Ni–N_{amido} bond length (1.907(3) Å) compares well with other Ni(II)-carboxamido complexes.[21,26,31-33,36] The average Ni–S bond distance (2.158(10) Å) is also within the range of Ni-S distances found in analogous Ni(II)-dicarboxamido-dithiolato species.[21,26,31-33]

Coordination of deprotonated carboxamido nitrogen to metal centers is readily indicated by the red-shift of the carbonyl stretching frequency (ν_{co}) of the complex with respect to the ν_{co} of the free ligand.[34] Complex **2** exhibits its ν_{co} at 1521 cm^{-1} compared to 1652 cm^{-1} for the free ligand $PhPepSH_4$. In MeCN, **2** exhibits a dark-red color arising from strong ligand-to-metal charge transfer absorption at 384 nm and a d-d band at 545 nm typical for Ni(II) complexes with dicarboxamido-dithiolato (N_2S_2) coordination.[21,26,31-33] The clean ^1H NMR spectrum of **2** in CD_3CN confirms that the square-planar geometry of **2** is retained in solution. Ligation of deprotonated carboxamido nitrogen to nickel in general provides exceptional stability to the 2+ and 3+ oxidation states.[21,31-33] In DMF, **2** displays an irreversible metal centered oxidation wave at 0.22 V (vs SCE). This value is more positive than the oxidation potential of other Ni(II)N_2S_2 complexes possibly due to the weaker donor strength of the aryl thiolate donors in **2** compared to the alkyl thiolates present in analogous complexes. Not surprisingly, **2** exhibits no reduction wave down to a potential of −1.8 V (vs SCE, DMF) due to the presence of strong σ-donors (carboxamido-N and thiolato-S) around the Ni(II) center.

(Et_4N)[Cu(neo)Ni(NpPepS)] (3)

The structure of **3** consists of a square-planar Ni(II) ion bridged to a distorted tetrahedral Cu(I) center via the thiolato-S donors of the $NpPepS^{4-}$ ligand frame (Figure 4). Close scrutiny of the Ni–N_{amido} and Ni–S bond distances in **3** (av: 1.899(4) and 2.1950(15) Å, respectively) reveals little changes from those noted for the Ni(II) monomer **1**. The Cu---Ni distance of **3** (3.074 Å) is somewhat longer than that of the Cu form of ACS/CODH (2.792 Å).[5] Steric constraints imposed by the $NpPepS^{4-}$ ligand frame are presumably responsible for the longer metal-metal distance compared with the enzyme value. The average Cu–N distance in **3** (2.047(4) Å) is typical of Cu(I)-neocuproine type complexes.[37] However, the two Cu–S distances are quite different with Cu–S1: 2.2670(16) and Cu–S2: 2.3198(16) Å. The distorted arrangement of the donor atoms around the Cu(I) center is further supported in the large deviation of the bond angles (N3–Cu–N4, 82.66(18)° and N3–Cu–S1, 129.79(14)°) from the ideal tetrahedral value of 109.5°. Similar distortion has also been observed in other sulfur-bridged Ni(II)-Cu(I) complexes.[25,27b]

Metallation of the sulfur ligands of the {Ni(NpPepS)} moiety in **3** is readily indicated by the blue shift of the ν_{co} value of the complex (1516 cm^{-1} compared to 1510 cm^{-1} in monomeric **1**). Enhanced charge donation by the carboxamido-N to compensate for the decreased donor strength of sulfur (following metallation by Cu) is presumably responsible for this blue-shift. Complex **3** is diamagnetic and exhibits a clean ^{1}H NMR spectrum. Although metallation of thiolate-S donors can alter the charge density at the Ni(II) center making the Ni(I) oxidation state more accessible,[23] **3** does not exhibit any observable redox wave down to –1.8 V (vs SCE, DMF). *Clearly, the Ni(I) state is not supported in this complex even with sulfur-metallation*. This lends further support toward a non-redox role for the Ni_d site in the enzyme.

(Et_4N)[Cu(neo)Ni(PhPepS)] (4)

The structure of the anion of the dinuclear Ni(II)-Cu(I) complex **4** is shown in Figure 5. Much like **3**, this complex also consists of a square-planar Ni(II) ion sulfur-bridged to a distorted tetrahedral Cu(I) center. The metric parameters of the NiN_2S_2 portion of **4** (av: Ni–N_{amido}, 1.9037(11) Å) are similar to that of monomer **2** except for slight elongation of the Ni–S bond distance (av: 2.1872(4) Å). Also, the bending of the aryl thiolate rings away from the NiN_2S_2 coordination plane is more noticeable in **4** compared to **2** as a result of the steric clash between the methyl groups of the neocuproine unit with the $PhPepS^{4-}$ ligand frame. This is reflected in the change of the C1–S1–Ni angle which is more compressed in **4** (99.06(5)°) than in **2** (106.53(11)°) and the highly distorted tetrahedral geometry about the Cu(I) center. For example, there is a significant difference in the two Cu–N bond lengths (Cu–N3: 2.0194(14) Å; Cu–N4: 2.0894(14) Å), the two Cu–S distances (Cu–S1: 2.2496(4) Å; Cu–S2: 2.3508(4) Å), and the bond angles range from 82.08(5)° (N3–Cu–N4) to 140.13(4)° (N3–Cu–S1). As a result the Cu---Ni bond distance of **4** (3.1435(2) Å) is longer than that observed in Cu-ACS. Like **3**, complex **4** exhibits a clean diamagnetic ^{1}H NMR spectrum and exhibits no Ni(II)/Ni(I) reduction wave in its cyclic voltammogram.

$(Et_4N)_2[Ni\{Ni(NpPepS)\}_2]$ (5)

An ORTEP drawing of the anion of the trinuclear Ni(II) complex $(Et_4N)_2[Ni\{Ni(NpPepS)\}_2]$ (**5**) is shown in Figure 6. The two terminal Ni(II) centers (designated as Ni_T; Ni1 and Ni3 in Figure 5) and the central Ni(II) center (designated as Ni_C; Ni2 in Figure 5) of **5** all lie in one extended plane in a slant chair configuration resulting from the orientation of the naphthalene rings. The two aryl sulfur rings of the $NpPepS^{4-}$ ligand frame fold in an up-down sequence and appear as railings for the $N_2Ni_TS_2$–Ni_C–$S_2Ni_TN_2$ platform. The Ni_T–N_{amido} and Ni_T–S bond distances in **5** (av: 1.880(3) and 2.1769 Å, respectively) are similar to those observed in **1** while the average Ni_C–S bond length (2.2368(10) Å) is slightly longer than those distances observed in similar Ni(II) trinuclear species.[21,38] Unique folding of the $NpPepS^{4-}$ ligand around the Ni_T centers in **5** is presumably responsible for this lengthening of the Ni_C–S bonds. Further comparison of the structural parameters of **5** with those of **1** reveal several differences in the coordination structure and ligand folding about the Ni(II) centers. For example, in **5**, the S1–Ni1–S2 bite angle is more compressed (86.85(4)°) compared to **1** (91.91(10)°) as a result of Ni_C coordination. Most notably, the 'butterfly' folding of the aryl sulfur rings in **5** allow the two adjacent rings on each $NpPepS^{4-}$ ligand frame to become much closer to each other compared to **1**. Finally, the C1–S1–Ni1 bond angle is considerably more closed in **5** (87.72(13)°) than in **1** (101.2(2)°).

The extremely low solubility of **5** in CD_3OD, CD_3CN and CD_2Cl_2 prevented the recording of its ^1H NMR spectrum although magnetic moment measurement (polycrystalline sample) confirmed its $S = 0$ spin state. As discussed below, dissolution of **5** in deuterated DMF or DMSO affords paramagnetic species due to solvent binding to Ni_C and such solutions exhibit broad NMR signals. Metallation of the sulfurs in **5** was also confirmed by the blue-shift of its ν_{CO} band (1538 cm^{-1}) compared to **1** (1510 cm^{-1}).

$(Et_4N)_2[Ni(DMF)_2\{Ni(NpPepS)\}_2]$ (6)

The structure of the anion of the DMF adduct **6** is shown in Figure 7. The binding of two molecules of DMF to Ni_C in **5** results in significant structural rearrangement. Major rearrangement occurs to accommodate the two additional DMF ligands coordinated to the Ni_C center in *cis* fashion by rotation of one of the $Ni_TN_2S_2$ units by ~ 90° to afford a distorted octahedral coordination unit around Ni_C. Although the average Ni–N_{amido} and Ni–S bond lengths of the Ni_T sites in **6** (1.893(3) and 2.1758(12) Å, respectively) remain unchanged (compared to **1** and **5**), the Ni_C–S bond distances (av: 2.4447(12) Å) increase significantly compared with **5** (av: 2.2368(10) Å) upon expansion of the coordination sphere. Additionally, this results in a longer Ni---Ni separation in **6** (3.374 Å) compared to **5** (3.2269(7) Å). The bending of the aryl sulfur rings of the $Ni_TN_2S_2$ units in **6** is also less pronounced (C1–S1–Ni1, 97.67(14)° compared to 87.72(13)° in **5**). A small *trans* influence of the coordinated DMF molecules in **6** is reflected in the two longer Ni_C–S bond distances (Ni2–S1, 2.4877(13) Å; Ni2–S3, 2.4495(12) Å). The increase in Ni_C–S could also arise from the increased metal-ligand electron repulsion in going from low-spin planar **5** ($S = 0$) to high-spin octahedral **6** ($S = 1$).

Complex **6** exhibits an additional ν_{CO} stretch at 1645 cm^{-1} due to the O-coordinated DMF molecules at the Ni_C center. The $S = 1$ spin state of **6** has been confirmed by measurement of the magnetic moment of the complex in the polycrystalline state (μ_{eff} = 2.87 μ_B at 298 K).

$(Et_4N)_2[Ni\{Ni(PhPepS)\}_2]$ (7)

At present we have not been able to grow good quality crystals of this complex for diffraction studies. However, microanalytical and spectroscopic data confirm an extended planar structure similar to that of complex **5**. This diamagnetic complex is more soluble in a variety of solvents than its analogue **5** and its clean ^1H NMR spectrum in CD_3CN is consistent with square-planar coordination around the three Ni(II) centers. The electronic absorption spectrum of **7** consists of several peaks in the 400-500 nm range arising from multiple ligand-to-metal charge transfer (LMCT) bands arising from the NiS_4 and NiN_2S_2 chromophores. As expected, the ν_{CO} band of **7** is shifted to higher energy (1538 cm^{-1}) compared to the monomeric complex **2** (1521 cm^{-1}).

$(Et_4N)_2[Ni(DMF)_2\{Ni(PhPepS)\}_2]$ (8)

The structure of the anion of the trinuclear complex **8** is shown in Figure 8. Much like the analogous trimer **6**, complex **8** also comprises two $Ni_TN_2S_2$ units coordinated to an octahedral Ni_C center (Ni2 in Figure 8). However, the $Ni_TN_2S_2$ moieties prefer to stay coplanar due to the decreased steric demands of the $PhPepS^{4-}$ ligand frame in **8**. This results in coordination of the two DMF molecules in a *trans* position at the Ni_C center. The average Ni_C–S and Ni_C–O bond distances of **8** (2.4475(16) and 2.063(5) Å, respectively) are very similar to those observed in **6** and other related complexes. When compared with **2**, the overall folding and metric parameters of the $PhPepS^{4-}$ ligand frame in **8** appear relatively unchanged with only a slight increase in the Ni_T–S bond length (av: 2.1723(18) Å) presumably due to metallation of sulfur by Ni_C. Collectively, the structures of **6** and **8** demonstrate that minor changes in the ligand design can alter the binding mode (e.g. *cis* vs *trans* coordination) of ligands and reactivity of metal centers in these model complexes. Complex **8** displays a strong ν_{CO} band at 1646 cm^{-1} due to the O-coordinated DMF ligands and its magnetic moment value (μ_{eff} = 2.89 μ_B at 298 K, polycrystalline sample) is consistent with an $S = 1$ ground state.

[Ni(terpy)Ni(NpPepS)] (9)

Although we have not completed structural studies on this model complex due to lack of suitable crystals, it has been thoroughly characterized by various spectroscopic techniques and its composition has been confirmed by microanalytical data. The blue-shift in the ν_{CO} band of complex **9** (1531 cm^{-1}) strongly supports the proposed dinuclear structure and the ESI-MS data support the presence of a $[Ni(terpy)]^{2+}$ moiety bound to a $[Ni(NpPepS)]^{2-}$ unit. Additional support for a five-coordinate Ni(II) center in **9** comes from the magnetic susceptibility studies (μ_{eff} = 3.02 μ_B at 298 K, polycrystalline sample). Since **9** exhibits an irreversible reduction at −1.13 V (vs SCE) in DMF, it is evident that the Ni(I) state is accessible in this model complex. Although the potential is still outside the biological range, this property of **9** allows one the opportunity to study the possibility of CO binding in the

reduced state (A_{red}-CO mimic). The results of such studies are discussed in detail in a forthcoming section.

[Ni(dppe)Ni(PhPepS)] (10)

The structure of the neutral dinuclear complex **10** is shown in Figure 9. In this Ni-Ni model, the two Ni(II) centers are connected via the two thiolato-S donors of the $PhPepS^{4-}$ ligand frame and both Ni centers exist in square-planar geometry. The spatial arrangement of the donor atoms of the NiN_2S_2 portion of this complex does not change significantly from that in the monomeric complex **2** and hence similar Ni–N_{amido} and Ni–S bond distances (av: 1.890(17) and 2.150(5) Å, respectively) are noted for **10**. The dihedral angle between the two Ni(II) square-planes in **10** is 111.4° and the Ni---Ni separation is 2.8255(4) Å (Ni---Ni in ACS/CODH = 3.00 Å).[6] Coordination of the Ni_p mimic to the two S-donors of the $PhPepS^{4-}$ results in a decrease bend of the aryl thiolate rings due to the shorter bite angle of the *cis*-dithiolato portion of the ligand frame (S1–Ni1–S2, 79.29(2)°). The bond angles about the bridged Ni_p center (Ni2 in Figure 9) in **10** also deviate from the ideal value (P1–Ni2–P2, 86.18(2)°; P1–Ni2– S1, 99.13(2)°) due to steric constraints imposed by the four phenyl groups of the diphosphine ligand. The average Ni–S and Ni–P bond distances of the Ni_p site in **10** (2.2384(6) and 2.1799(6) Å, respectively) are similar to those found in other dinuclear Ni complexes with P_2S_2 coordination spheres.[19,22]

The dinuclear structure of **10** is readily identified by the blue-shift of the ν_{CO} to 1538 cm^{-1} from 1521 cm^{-1} in case of **2**. The two square-planar Ni(II) centers of **10** give rise to a diamagnetic species that exhibits a clean ^1H NMR spectrum in $CDCl_3$.

Reactivity with 1,10-phenanthroline

In some of the earliest studies on ACS/CODH (before any structural analysis), Lindahl and coworkers showed that a portion of the Ni at the A-cluster site is labile and easily removed with the bidentate chelator 1,10-phenanthroline (phen).[11b] This removal of “labile Ni” by phen completely inhibits the ACS activity but leaves the CODH activity intact. The phen-treated enzyme also displays no NiFeC EPR signal. We were therefore curious to determine whether the sulfur-bridged Ni in the model complexes such as **6, 8** and **10** can be removed with phen. Previous studies on a trinuclear model complex reported by Darensbourg and coworkers, namely $[\{(BME\text{-}DACO)Ni\}_2Ni]Br_2$, have shown that the Ni(II) center coordinated by four metallosulfur moieties from the NiN_2S_2 units in the complex is indeed removed by phen.[23] However, the absence of key carboxamido groups in the NiN_2S_2 fragments in these trinuclear species, as well as the lack of phen reactivity with a trinuclear complex similar to **6** (and **8**) with carboxamido coordination synthesized by Hegg and coworkers[21] prompted us to study the phen reactivity with our complexes.

Titration of solutions of **6** or **8** in DMF with phen results in immediate removal of the central Ni (Ni_C) ions in both these trinuclear species. The reaction can be followed by monitoring the electronic absorption spectrum. As shown in Figure 10, the spectrum completely stops changing only after addition of 3 mol equiv of phen to **6** suggesting formation of $[Ni(phen)_3]^{2+}$ and 2 mol equiv of the monomer **1**.[27b] Similar results were obtained with complex **8**. Since no further change is observed upon addition of a large excess (~ 100 mol

equiv) of phen to these solutions, it is evident that the Ni(II) centers in the Ni_d mimics **1** and **2** are strongly coordinated to their dicarboxamido-dithiolato ligand frames and are resistant to removal by phen.

The reactivity of phen with the dinuclear model **10** is slightly different from its trinuclear counterparts **6** and **8**.[27a] Addition of phen to a solution of **10** in CH_2Cl_2 does remove the sulfur-bridged Ni_p model site in this complex resulting in the formation of **2**, $[Ni(phen)_3]^{2+}$, and free dppe in solution. However, the removal of Ni_p in **10** requires excess phen (~ 25 mol equiv) and takes nearly 35 min to reach the end point (beyond which no further change occurs in the electronic absorption spectrum, Figure 11). The observed pseudo first order rate constant (k_{obs}) for the phen removal of Ni_p in dimer **10** is 1.50×10^{-4} s^{-1}. The slower phen reactivity of **10** compared to **6** and **8** presumably arises from the more stable square-planar low-spin nature of the Ni_p site in **10** as opposed to the high-spin octahedral Ni_C centers in **6** and **8**. Interestingly, treatment of the Ni-Cu dimers **3** and **4** with phen does not result in any reaction. However, addition of the Cu(I) specific chelator neocuproine to **3** and **4** affords the respective monomers **1** and **2** and $[Cu(neo)_2]^+$. Neocuproine exhibits no reaction with the Ni centers of **6, 8**, or **10**. Collectively, the phen reactivity of the Ni complexes **6, 8**, and **10** lends further support to the notion that the “labile Ni” in the enzyme originates from the M_p site and *not* the Ni_d site.[11,12] The results also provide indirect evidence in favor of Ni at the M_p site of the Acluster of *catalytically active* ACS/CODH.

Reactivity of Ni-Cu Models

The Cu(I) sites in all the synthetic models reported so far exhibit no affinity toward CO. For example, the dinuclear models synthesized by Riordan and coworkers undergo rupture of the $(\mu\text{-}SR)_2$ bridge and breakdown of the dinuclear structure upon reaction with CO.[25] The Ni-Cu dinuclear complex, $[\{P(i\text{Pr})_3Cu\}\{NiS_2N'_2\}]^-$, synthesized by Rauchfuss and coworkers with a coordinatively unsaturated Cu(I) center, does not exhibit any CO binding.[24] Although some of these models utilize Ni(II)-diamino-dithiolato complexes as the Ni_d synthon and hence lack crucial Ni(II)-carboxamido-N interaction(s),[25] the consistent inertness of the Cu(I) centers in these model complexes indicates a non-catalytic role for Cu in ACS/CODH.

The Ni-Cu models of the present work namely, **3** and **4**, consist of Ni_d synthons that include carboxamido ligation to the Ni(II) center. Both these models exhibit no CO binding to either metal center nor is any breakdown of the Cu-$(\mu\text{-}SR)_2$-Ni core observed upon passage of CO through the solutions of these complexes. No breakdown of the Cu- $(\mu\text{-}SR)_2$-Ni core is observed upon treatment with excess phen either. Clearly, the dinuclear structures are very stable and are in accord with results of previous experiments showing Cu(I) ion as a stronger binder to metallosulfur donors compared to Ni(II) and Zn(II) ions.[23] Although the lack of reactivity of the Cu(I) centers of **3** and **4** toward CO could simply arise from coordinative saturation (both tetrahedrally coordinated), it is important to note that exposure to CO does not cause any break in the Cu-S bridge to provide a binding site for CO. This indicates that Cu(I) binds the thiolato sulfurs of the Ni_d site quite strongly and hence the presence of Cu at the M_p site in Drennan’s structure could be a consequence of binding of adventitious metal ions present in the crystallization buffers.[11] Indeed, in a recent paper, Darensbourg and coworkers have examined the metal ion affinity of an analogous NiN_2S_2 thiolato complex,

([(BMEDACO) Ni]), and the results indicate that the affinity decreases in the order Cu(I)>Ni(II)>Zn(II).[23]

Reactivity of Ni-Ni Models

Since one of the steps of the proposed ACS mechanism invokes the formation of a Ni(I)-CO species, responsible for the NiFeC EPR signal, we have studied the redox properties and CO-affinities of the bridged Ni(II) centers in **6** and **8-10**. The redox behaviors of the models of the Ni_d sites reported so far suggest that the Ni_d site of the A-cluster is unlikely to participate in any redox process during catalysis and in turn imply that the Ni_p site is a candidate for reduction and CO binding during the ACS catalyzed reaction.[19-25] The Ni_C centers of the trinuclear species **6** and **8** are ligated to four metallosulfur ligands and hence resemble the Ni_p site to a great extent. Both these models can be chemically reduced with reductants like $Na_2S_2O_4$ and $NaBH_4$ at low temperature (−40 °C) to afford EPR-active species. The X-band EPR spectrum of the reduced species $\mathbf{6_{red}}$ in DMF glass (100 K) consists of an axial EPR signal (g = 2.33, 2.09) while that of $\mathbf{8_{red}}$ is more rhombic (g = 2.25, 2.12, 2.07). Since **1** and **2** cannot be reduced by $Na_2S_2O_4$ or $NaBH_4$ (no EPR signal), it is evident that the $Ni(II)_C$ centers in the trinuclear complexes undergo reduction. The similarity of the EPR spectra of $\mathbf{6_{red}}$ and $\mathbf{8_{red}}$ with those of other $[Ni(I)L_4]$ species leads us to propose that the coordination geometry about the $Ni(I)_C$ center in these reduced complexes is distorted tetrahedral.[39]

Passage of CO into DMF solutions of $\mathbf{6_{red}}$ and $\mathbf{8_{red}}$ results in the formation of their CO-adducts that exhibit intense ν_{CO} bands in their solution IR spectra at 1960 and 1971 cm^{-1}, respectively. These ν_{CO} values are consistent with terminal coordination of CO to the $Ni(I)_C$ centers of $\mathbf{6_{red}}$**-CO** and $\mathbf{8_{red}}$**-CO** much like that proposed in ACS. The reduced $Ni(I)S_4$ complex $[Ni(tpttd)]^-$ (tpttd = 2,2,11,11-tetraphenyl-1,5,8,12-tetrathiadodecane) with two alkyl thiolato-S donors also binds CO in a similar manner and exhibits its ν_{CO} value at 1940 cm^{-1}.[40] The ν_{CO} values for $\mathbf{6_{red}}$**-CO** and $\mathbf{8_{red}}$**-CO** are lower than that recorded for the enzyme (1996 cm^{-1}). This red shift presumably arises from the enhanced electron density at the Ni(I) centers ligated by *four* metallosulfur donors (instead of the *three* observed in the enzyme) which in turn promotes more π back donation to the π* orbital of CO. The reduced species and their CO-adducts are moderately stable at low temperatures. All efforts to isolate solids from the reaction mixtures have so far met with little success.

The Ni-Ni model complexes **9** and **10** provided the opportunity to study the reactions of CO with Ni(I) centers at modeled M_p sites (with different coordination geometries) as more accurate mimics of the bimetallic A-cluster subsite.[27a] When complex **9** with N_3S_2 donor set at the Ni_p site is reduced with $Na_2S_2O_4$ in DMF, the product exhibits an axial EPR spectrum with g = 2.23 and 2.12 (Figure 12, top panel). This spectrum is nearly identical to the EPR spectra of $[Ni^I(terpy)(SR)_2]^-$ species with distorted trigonal bipyramidal geometry.[41] It is therefore clear that $\mathbf{9_{red}}$ retains its dinuclear structure and that the Ni_p center in **9** is reduced to the Ni(I) state. Passage of CO through the solution of $\mathbf{9_{red}}$ in DMF affords $\mathbf{9_{red}}$**-CO** that exhibits a strong ν_{CO} band in its solution IR spectrum at 2044 cm^{-1}.

Since both **1** and **9** do not show any affinity toward CO, one can easily conclude that the Ni(I) center binds CO in **9_{red}-CO**. The EPR spectrum of **9_{red}-CO** is rhombic compared to **9_{red}** with g = 2.22, 2.13, and 2.02 (Figure 12, bottom panel) and resembles the EPR spectra of $[Ni^{I}(terpy)(SR)_2(CO)]^-$ species reported by this group.[41] For example, the Ni(I) complex, $[Ni^{I}(terpy)(C_6F_5S)_2(CO)]^-$ exhibits a rhombic EPR signal in DMF glass with g = 2.20, 2.15, 2.02 and displays ν_{CO} band at 2045 cm^{-1}.[41c] These data clearly indicate that the Ni(I) center in **9_{red}-CO** exists in a distorted octahedral geometry and the CO is bound in a terminal fashion. The reduced complex, **9_{red}**, and its CO-adduct, **9_{red}-CO**, are moderately stable at low temperatures and decompose rapidly at room temperature. Prolonged passage of CO through DMF solutions of **9_{red}** also affords $[Ni^{I}(terpy)(CO)_2]^+$.

Since the Ni_p site of ACS exists in a planar geometry in the structurally characterized (as isolated) enzyme,[6,7] the modeled Ni_p site of **10** was a more attractive target to study. It was expected that phosphine coordination to Ni_p in **10** would make the Ni(I) oxidation state accessible and result in a more stable CO-adduct. Both expectations have been met with **10**. Complex **10** can be readily reduced by reductants such as $NaBH_4$ and cobaltocene. The X-band EPR spectrum of **10_{red}** is consistent with a distorted tetrahedral Ni(I) center with P_2S_2 coordination and the resulting g values are close to 2.00 with significant hyperfine splitting originating from the two non-equivalent ^{31}P nuclei of the dppe ligand frame.[22,42] The reduced species is quite stable at room temperature. Under anaerobic condition, one can monitor the reduction of **10** to **10_{red}** in CH_2Cl_2 with the use of one equiv of cobaltocene. Reaction of one equiv of cobaltocene with **10** affords **10_{red}**, the species exhibiting the EPR spectrum. The violet color of **10** changes to light red-brown upon reduction. When the solution of **10_{red}** in CH_2Cl_2 is exposed to air, it is immediately reoxidized to **10** in nearly quantitative yield (Figure 13). This confirms that the $(\mu\text{-}SR)_2$ bridge remains intact during reduction.

Passage of CO through a solution of **10_{red}** in CH_2Cl_2 (or DMF) gives rise to the CO-adduct **10_{red}-CO** that exhibits a strong ν_{CO} band in its IR spectrum at 1997 cm^{-1}, consistent with terminally bound CO to the $Ni(I)_p$ center. Complete removal of the solvent affords a dark red solid which also displays the same ν_{CO} band in KBr matrix (supporting information).[43] Since the ν_{CO} value of **10_{red}-CO** is very close to the enzyme value of 1996 cm^{-1}, it is reasonable to conclude that the Ni_p center in the enzyme binds CO in the +1 oxidation state. In $[\{Ni(CO)_2\}\{NiS_2N'_2\}]^{2-}$ (Figure 2a), two molecules of CO are bound to a Ni(0) center in terminal fashion.[24] This Ni_p mimic displays two ν_{CO} bands at 1948 and 1866 cm^{-1}. Holm and coworkers have reported a Ni(0) complex [Ni(bpy)$(CO)_2$] (bpy = 2,2′-bipyridine) which exhibits ν_{CO} bands at 1872 and 1973 cm^{-1} (KBr matrix).[44] Since these ν_{CO} values are all lower than that displayed by **10_{red}-CO**, it is evident that the latter species does contain Ni(I) and not Ni(0) at the Ni_p site. As mentioned above, the Ni_d site of **10** is quite resistant to reduction. Indeed, the ν_{CO} values arising from the ligated carboxamido groups at the Ni_d sites of **10** and **10_{red}-CO** are very close to each other and further support the presence of Ni(II) at the Ni_d site in **10_{red}-CO**.

The EPR spectrum of **10_{red}-CO** in DMF glass is rhombic with g_1 = 2.20, g_2, = 2.12, g_3 = 2.05; each line is split into a triplet from coupling to two non-equivalent $_{31}P$ nuclei (Figure

14). This spectrum resembles the EPR spectrum of $[Ni(psnet)]^+$, a structurally characterized five-coordinate complex with distorted square pyramidal P_2S_2N ligation to a Ni(I) center.[42a] The magnetic hyperfine interaction of ^{31}P nuclei with an unpaired electron of Ni(I) has been shown to be very susceptible to the coordination geometry around the metal center.[42b] For example, the EPR spectrum of the tetrahedral Ni(I) complex $[Ni(PMe_3)_4]^+$ (av. P-N-P angle = 109°) consists of an isotropic broad resonance with $g = 2.12$ with no ^{31}P hyperfine coupling[45] while the Ni(I) complex $[Ni(psnet)]_+$ with distorted square pyramidal structure exhibits a rhombic EPR signal with $g_1 = 2.21$, $g_2 = 2.13$ and $g_3 = 2.01$ and $a_1 = 45$ G, $a_2 = 40$ G and $a_3 = 44$ G respectively.[42a] In the present case, three distinct ^{31}P hyperfine couplings with a values in the range of 30-60 G are noted with $\mathbf{10_{red}}$**-CO** (Figure 14). We therefore assign a $\{Ni^{I}P_2S_2(CO)\}–(\mu\text{-}SR)_2–\{Ni^{II}(N_2S_2)\}$ formulation to $\mathbf{10_{red}}$**-CO**.

Recently, three groups have reported sulfur-bridged dinuclear Ni complexes with P_2S_2 coordination[19,20a,22] at the bridged Ni center (Ni_p mimic) that exhibit low Ni(I)/Ni(II) redox potentials.[20,22] Unfortunately, very little spectroscopic data are currently available on the CO adducts of these complexes in the reduced state. Complex **10** deserves attention in this regard as the first structurally characterized Ni-Ni model that includes dicarboxamido-dithiolato ligation (Ni_d mimic) to a bridged Ni(II) center that (i) can be reduced to the Ni(I) state and (ii) binds CO in the reduced state (Ni_p mimic) much like that proposed for the A-cluster of ACS/CODH.

In the absence of the Fe_4S_4 portion of the A-cluster in the sulfur-bridged Ni-Ni models, it is impossible to assess the effect(s) of the iron-sulfur cluster on the chemical and redox properties of the Ni_p center. Although recent studies have indicated that electron flow to and from the Fe_4S_4 cluster is too slow compared to the rate of methyl transfer,[46] the proposed mechanisms of ACS activity mostly involve redox changes at the Fe_4S_4 cluster during key steps of the catalytic cycle.[5,6,47,48] Theoretical studies suggest that the Ni(0) state[49] is only stabilized by either removal of the cluster[15] or by the presence of a neighboring reduced iron-sulfur cluster $[Fe_4S_4]^{1+}$ ($S = ½$).[48] Clearly, the next generation models of the ACS A-cluster have to incorporate the Fe_4S_4 cluster in order to address these issues.[47] Such attempts are in progress in this laboratory at this time.[50]

Conclusions

The results of the modeling work reported here reveal valuable insight into the novel A-cluster site involved in acetyl CoA synthesis by ACS/CODH. For example, it is quite evident that coordination of both carboxamido nitrogen and thiolato sulfur stabilizes the Ni(II) state to a great extent (like in **1** and **2**) and hence the Ni_d site in the enzyme is not expected to participate in any redox chemistry. Binding of potential substrates such as CO at this site is also unlikely. Furthermore, Ni(II) centers bridged to metallosulfur moieties (Ni_p mimics) appear quite capable of binding substrates like CO when in the reduced Ni(I) state but not in the Ni(II) state. The IR spectra of such CO-adducts exhibit ν_{CO} bands in the range 1960-2044 cm^{-1}, indicating terminal Ni(I)-CO coordination similar to that proposed in the enzyme (ν_{CO} = 1996 cm^{-1}). Since the Ni-Ni models of this work (such as **9** and **10**) are devoid of the strong dipolar coupling of the Ni_p site to the Fe_4S_4 cluster, the EPR spectra of the CO-adducts like $\mathbf{10_{red}}$**-CO** do not resemble the NiFeC EPR signal. The removal of Ni_p sites

from selected models by phen provides strong evidence in favor of Ni_p being the source of "labile Ni" in the enzyme. No reactivity toward CO has been noted with the dinuclear Ni-Cu models (**3** and **4**). Collectively, these observations lend support to the present notion that the M_p site in catalytically active ACS/CODH is occupied by Ni.

Supplementary Material

Refer to Web version on PubMed Central for supplementary material.

Acknowledgments

T. C. H. received financial support from the NIH IMSD grant GM58903.

References

1. (a) Ragsdale SW. Crit Rev Biochem Mol Biol. 2004; 39:165–195. [PubMed: 15596550] (b) Ragsdale SW, Kumar M. Chem Rev. 1996; 96:2515–2539. [PubMed: 11848835]
2. Lindahl PA. Biochemistry. 2002; 41:2097–2105. [PubMed: 11841199]
3. Wood, HG.; Ljungdahl, LG. Variation in Autotrophic Life. Academic Press; New York, NY: 1991.
4. Huber C, Wächtershäuser G. Science. 1997; 276:245–247. [PubMed: 9092471]
5. Doukov TI, Iverson TM, Seravalli J, Ragsdale SW, Drennan CL. Science. 2002; 298:567–572. [PubMed: 12386327]
6. Darnault C, Volbeda A, Kim EJ, Legrand P, Vernède X, Lindahl PA, Fontecilla-Camps JC. Nat Struct Biol. 2003; 10:271–279. [PubMed: 12627225]
7. Svetlitchnyi V, Dobbek H, Meyer-Klaucke W, Meins T, Thiele B, Römer P, Huber R, Meyer O. Proc Natl Acad Sci USA. 2004; 101:446–451. [PubMed: 14699043]
8. (a) George SJ, Seravalli J, Ragsdale SW. J Am Chem Soc. 2005; 127:13500–13501. [PubMed: 16190705] (b) Seravalli J, Kumar M, Ragsdale SW. Biochemistry. 2002; 41:1807–1819. [PubMed: 11827525] (c) Xia J, Hu Z, Popescu CV, Lindahl PA, Münck E. J Am Chem Soc. 1997; 119:8301–8312.(d) Ragsdale SW, Wood HG, Antholine WE. Proc Natl Acad Sci USA. 1985; 82:6811. [PubMed: 2995986]
9. Chen J, Huang S, Seravalli J, Gutzman H Jr, Swartz DJ, Ragsdale SW, Bagley KA. Biochemistry. 2003; 42:14822–14830. [PubMed: 14674756]
10. (a) Tan XS, Sewell C, Lindahl PA. J Am Chem Soc. 2002; 124:6277–6284. [PubMed: 12033855] (b) Barondeau DP, Lindahl PA. J Am Chem Soc. 1997; 119:3959–3970.
11. (a) Bramlett MR, Tan X, Lindahl PA. J Am Chem Soc. 2003; 125:9316–9317. [PubMed: 12889960] (b) Shin W, Lindahl PA. J Am Chem Soc. 1992; 114:9718–9719.
12. Seravalli J, Xiao Y, Gu W, Cramer SP, Antholine WE, Krymov V, Gerfen GJ, Ragsdale SW. Biochemistry. 2004; 43:3944–3955. [PubMed: 15049702]
13. (a) Funk T, Gu W, Friedrich S, Wang H, Gencic S, Grahame DA, Cramer SP. J Am Chem Soc. 2004; 126:88–95. [PubMed: 14709073] (b) Gencic S, Grahame DA. J Biol Chem. 2003; 278:6101–6110. [PubMed: 12464601]
14. Webster CE, Darensbourg MY, Lindahl PA, Hall MB. J Am Chem Soc. 2004; 126:3410–3411. [PubMed: 15025453]
15. (a) Brunold TC. J Biol Inorg Chem. 2004; 9:533–541. [PubMed: 15221480] (b) Schenker RP, Brunold TC. J Am Chem Soc. 2003; 125:13962–13963. [PubMed: 14611224]
16. Peters JW, Stowell MHB, Soltis M, Finnegan MG, Johnson MK, Rees DC. Biochemistry. 1997; 36:1181–1187. [PubMed: 9063865]
17. (a) Harrop TC, Mascharak PK. Acc Chem Res. 2004; 37:253–260. [PubMed: 15096062] (b) Mascharak PK. Coord Chem Rev. 2002; 225:201–214.(c) Nagashima S, Nakasako M, Dohmae N, Tsujimura M, Takio K, Odaka M, Yohda M, Kamiya N, Endo I. Nat Struct Biol. 1998; 5:347–351.

[PubMed: 9586994] (d) Huang W, Jia J, Cummings J, Nelson M, Schneider G, Lindqvist Y. Structure. 1997; 5:691–699. [PubMed: 9195885]

18. (a) Barondeau DP, Kassmann CJ, Bruns CK, Tainer JA, Getzoff ED. Biochemistry. 2004; 43:8038–8047. [PubMed: 15209499] (b) Wuerges J, Lee J-W, Yim Y-I, Yim H-S, Kang S-O, Carugo KD. Proc Natl Acad Sci USA. 2004; 101:8569–8574. [PubMed: 15173586]
19. Rao PV, Bhaduri S, Jiang J, Holm RH. Inorg Chem. 2004; 43:5833–5849. [PubMed: 15360232]
20. (a) Krishnan R, Riordan CG. J Am Chem Soc. 2004; 126:4484–4485. [PubMed: 15070343] (b) Krishnan R, Voo JK, Riordan CG, Zahkarov L, Rheingold AL. J Am Chem Soc. 2003; 125:4422–4423. [PubMed: 12683803]
21. Hatlevik Ø, Blanksma MC, Mathrubootham V, Arif AM, Hegg EL. J Biol Inorg Chem. 2004; 9:238–246. [PubMed: 14735332]
22. Wang Q, Blake AJ, Davies ES, McInnes EJL, Wilson C, Schröder M. Chem Commun. 2003:3012–3013.
23. Golden ML, Rampersad MV, Reibenspies JH, Darensbourg MY. Chem Commun. 2003:1824–1825.
24. Linck RC, Spahn CW, Rauchfuss TB, Wilson SR. J Am Chem Soc. 2003; 125:8700–8701. [PubMed: 12862445]
25. Harrop TC, Mascharak PK. Coord Chem Rev. 2005; 249:3007–3024.
26. Harrop TC, Olmstead MM, Mascharak PK. Inorg, Chim Acta. 2002; 338:189–195.
27. (a) Harrop TC, Olmstead MM, Mascharak PK. J Am Chem Soc. 2004; 126:14714–14715. [PubMed: 15535684] (b) Harrop TC, Olmstead MM, Mascharak PK. Chem Commun. 2004:1744–1745.
28. Gill NS, Taylor FB. Inorg Synth. 1967; 9:136–143.
29. (a) Healy PC, Pakawatchai C, White AH. J Chem Soc Dalton Trans. 1985:2531–2539.(b) Rao CP, Dorfman JR, Holm RH. Inorg Chem. 1986; 25:428–439.(c) Anderson OP, Brito KK, Laird SK. Acta Cryst. 1990; C46:1600–1603.
30. Judge JS, Reiff WM, Intille GM, Ballway P, Baker WA Jr. J Inorg Nucl Chem. 1967; 29:1711–1716.
31. (a) Krüger H-J, Peng G, Holm RH. Inorg Chem. 1991; 30:734–742.(b) Krüger H-J, Holm RH. Inorg Chem. 1987; 26:3645–3647.
32. Dutton JC, Fallon GD, Murray KS. Chem Lett. 1990:983–986.
33. Hanss J, Krüger H-J. Angew Chem Int Ed. 1998; 37:360–363.
34. Marlin DS, Mascharak PK. Chem Soc Rev. 2000; 29:69–74.
35. Smeets WJJ, Spek AL, Henderson RK, Bouwman E, Reedijk J. Acta Cryst Sect C. 1997; C53:1564–1566.
36. Chapman RL, Vagg RS. Inorg Chim Acta. 1979; 33:227–234.
37. Pallenberg AJ, Koenig KS, Barnhart DM. Inorg Chem. 1995; 34:2833–2840.
38. (a) Farmer PJ, Solouki T, Mills DK, Soma T, Russell DH, Reibenspies JH, Darensbourg MY. J Am Chem Soc. 1992; 114:4601–4605.(b) Turner MA, Driessen WL, Reedijk J. Inorg Chem. 1990; 29:3331–3335.
39. (a) Craft JL, Mandimutsira BS, Fujita K, Riordan CG, Brunold TC. Inorg Chem. 2003; 42:859–867. [PubMed: 12562200] (b) Musie G, Farmer PJ, Tuntulani T, Reibenspies JH, Darensbourg MY. Inorg Chem. 1996; 35:2176–2183. [PubMed: 11666411]
40. Yamamura T, Sakurai S, Arai H, Miyamae H. J Chem Soc Chem Commun. 1993:1656–1658.
41. (a) Marganian CA, Vazir H, Baidya N, Olmstead MM, Mascharak PK. J Am Chem Soc. 1995; 117:1584–1594.(b) Baidya N, Olmstead MM, Whitehead JP, Bagyinka C, Maroney MJ, Mascharak PK. Inorg Chem. 1992; 31:3612–3619.(c) Baidya N, Olmstead MM, Mascharak PK. Inorg Chem. 1991; 30:929–937.
42. (a) James TL, Cai L, Muetterties MC, Holm RH. Inorg Chem. 1996; 35:4148–4161. [PubMed: 11666623] (b) Kim JS, Reibenspies JH, Darensbourg MY. J Am Chem Soc. 1996; 118:4115–4123. (c) James TL, Smith DM, Holm RH. Inorg Chem. 1994; 33:4869–4877.(d) Bowmaker GA, Boyd PDW, Campbell GK. Inorg Chem. 1982; 21:2403–2412.
43.

The red solid is moderately stable under anaerobic conditions, however, it decomposes slowly in solution and to date, we have not been able to characterize it by structural studies. The EPR spectrum of a solution of the freshly isolated red solid in DMF (same as Figure 14) confirms that the solid is indeed **10_{red}-CO**.

44. Tucci GC, Holm RH. J Am Chem Soc. 1995; 117:6489–6496.
45. Gleizes A, Dartiguenave M, Dartiguenave Y, Galy J, Klein HF. J Am Chem Soc. 1977; 99:5187–5189.
46. Tan X, Sewell C, Yang Q, Lindahl PA. J Am Chem Soc. 2003; 125:318–319. [PubMed: 12517128]
47. Hegg EL. Acc Chem Res. 2004; 37:775–783. [PubMed: 15491124]
48. Amara P, Volbeda A, Fontecilla-Camps JC, Field MJ. J Am Chem Soc. 2005; 127:2776–2784. [PubMed: 15725036]
49. Lindahl PA. J Biol Inorg Chem. 2004; 9:516–524. [PubMed: 15221478]
50. In a recent paper, Holm and coworkers have reported the results of such an attempt. However, only complexes of the thiolato-bridged $[Fe_4S_4]$-NiL type have been isolated. See: Rao PV, Bhaduri S, Jiang J, Hong D, Holm RH. J Am Chem Soc. 2005; 127:1933–1945. [PubMed: 15701028]

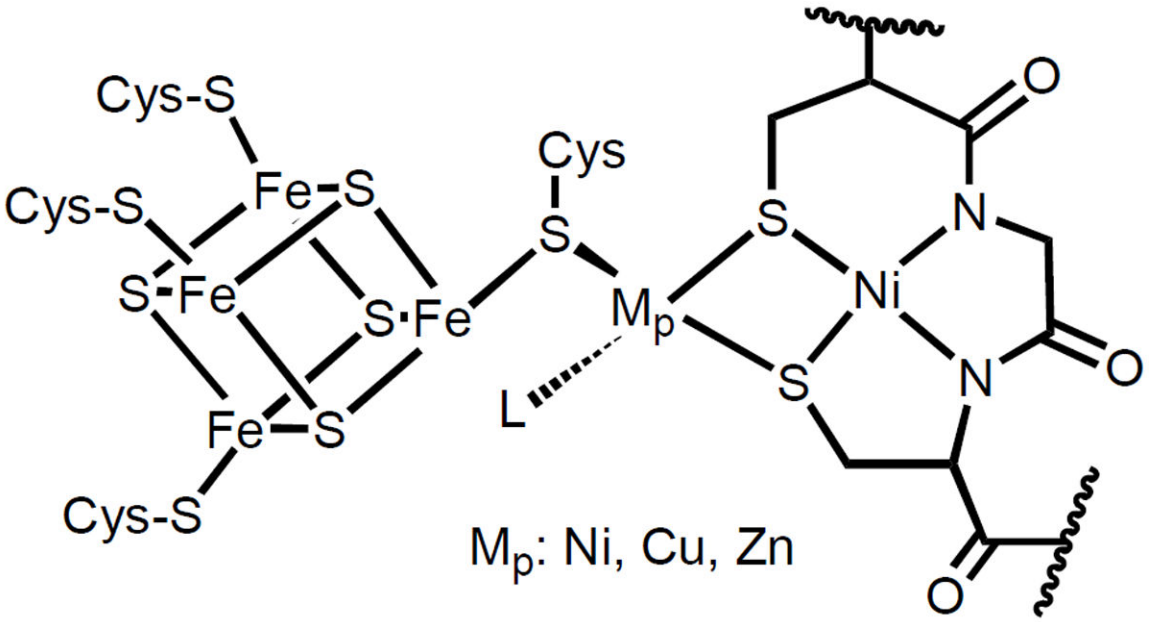

Figure 1.

Schematic of the A-cluster site of ACS/CODH from *Moorella thermoacetica*. M_p: Ni(II), Cu(I), or Zn(II); L is a non-protein ligand.

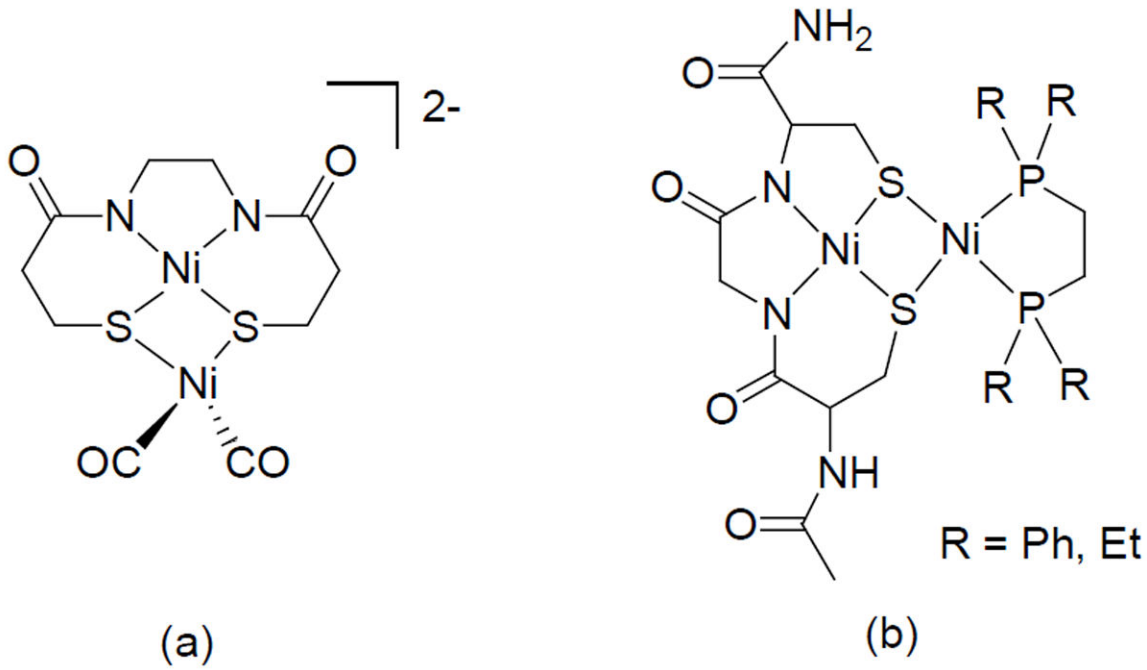

Figure 2.
Structures of (a) $[\{Ni(CO)_2\}\{NiS_2N'_2\}]^{2-}$ and (b) [Ni(CGC)Ni(dRpe)]

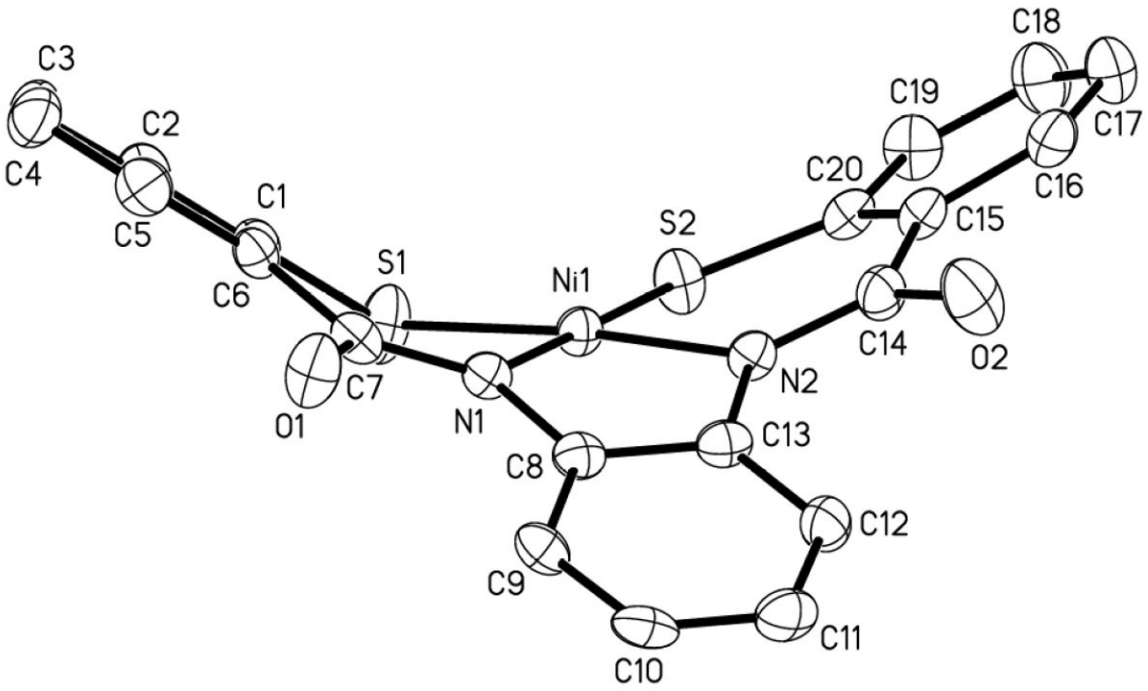

Figure 3.

ORTEP diagram of the anion of $[Ni(PhPepS)]^{2-}$ (anion of **2**) (50 % probability) with the atom-labeling scheme. H atoms are omitted for the sake of clarity.

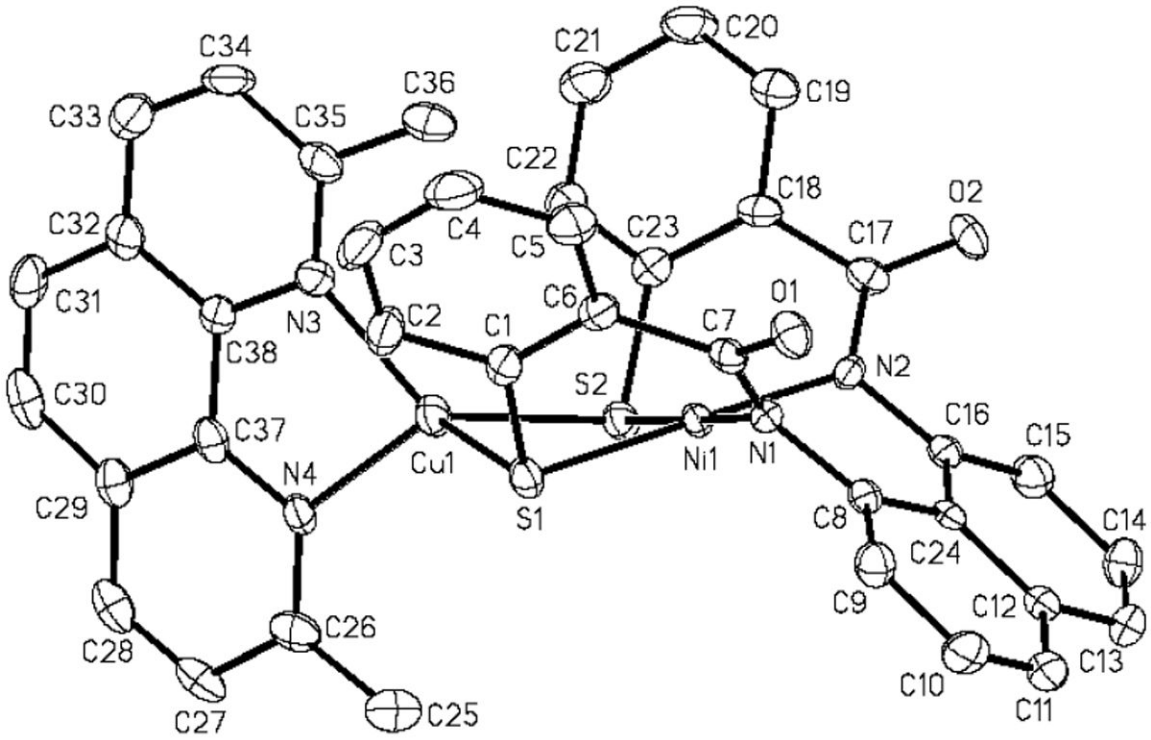

Figure 4.

ORTEP diagram of $[Cu(neo)Ni(NpPepS)]^{-}$ (anion of **3**) (50 % probability) with the atom-labeling scheme. H atoms are omitted for the sake of clarity.

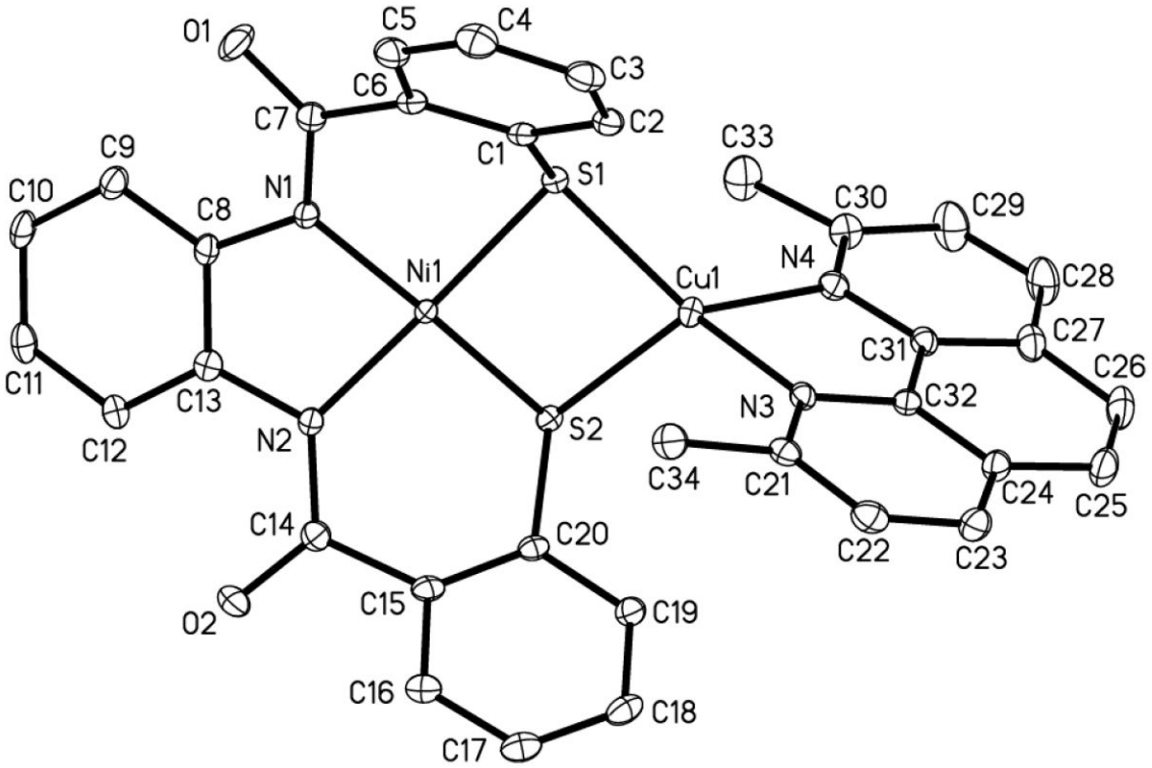

Figure 5.

ORTEP diagram of $[Cu(neo)Ni(PhPepS)]^{-}$ (anion of **4**) (50 % probability) with the atom-labeling scheme. H atoms are omitted for the sake of clarity.

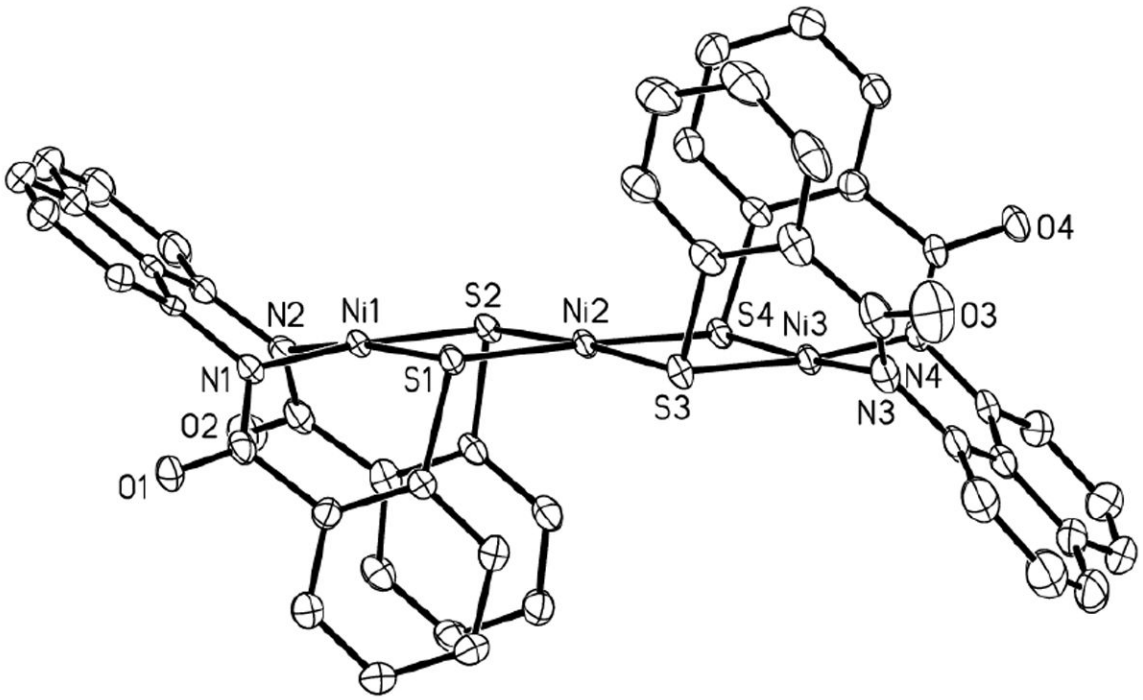

Figure 6.

ORTEP diagram of $[Ni\{Ni(NpPepS)\}_2]^{2-}$ (anion of **5**) (50 % probability) with the atom-labeling scheme. H atoms are omitted for the sake of clarity.

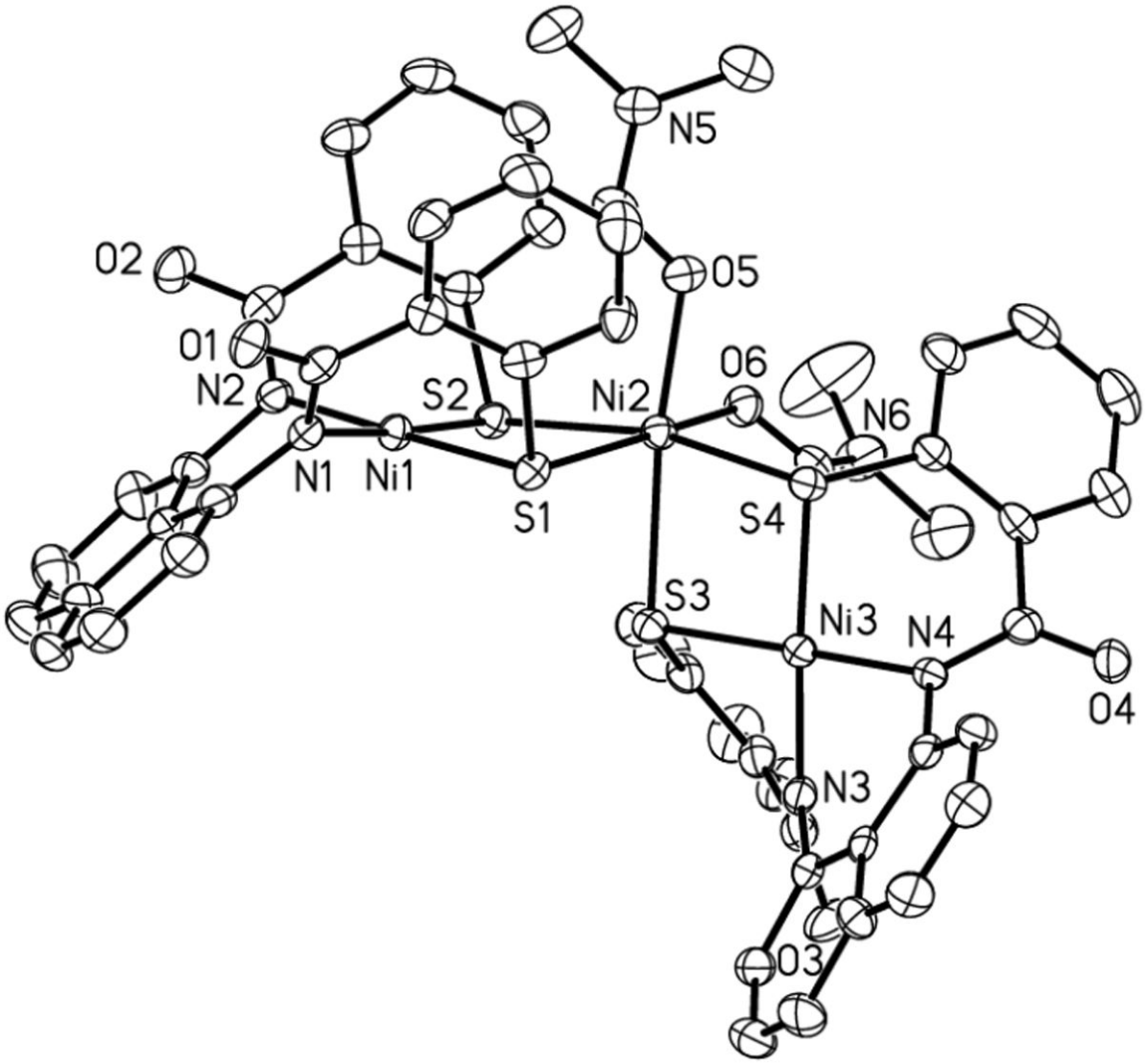

Figure 7.

ORTEP diagram of $[Ni(DMF)_2\{Ni(NpPepS)\}_2]^{2-}$ (anion of **6**) (50 % probability) with the atom-labeling scheme. H atoms are omitted for the sake of clarity.

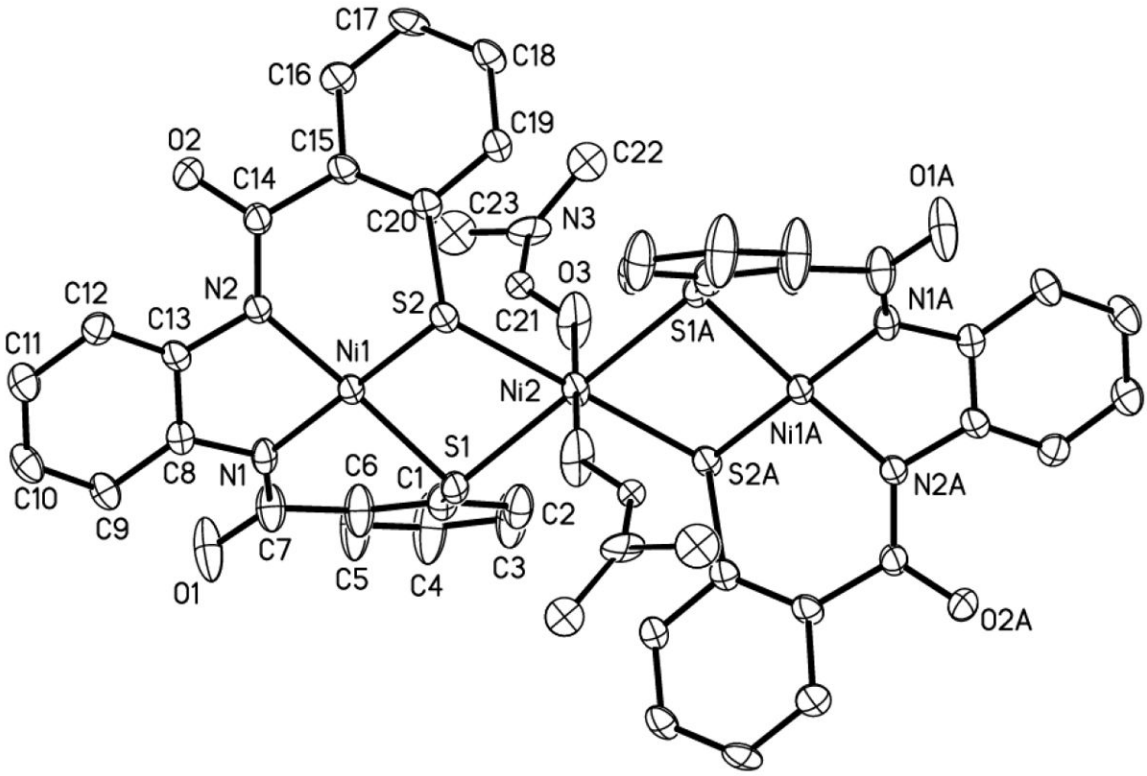

Figure 8.

ORTEP diagram of $[Ni(DMF)_2\{Ni(PhPepS)\}_2]^{2-}$ (anion of **8**) (50 % probability) with the atom-labeling scheme. H atoms are omitted for the sake of clarity.

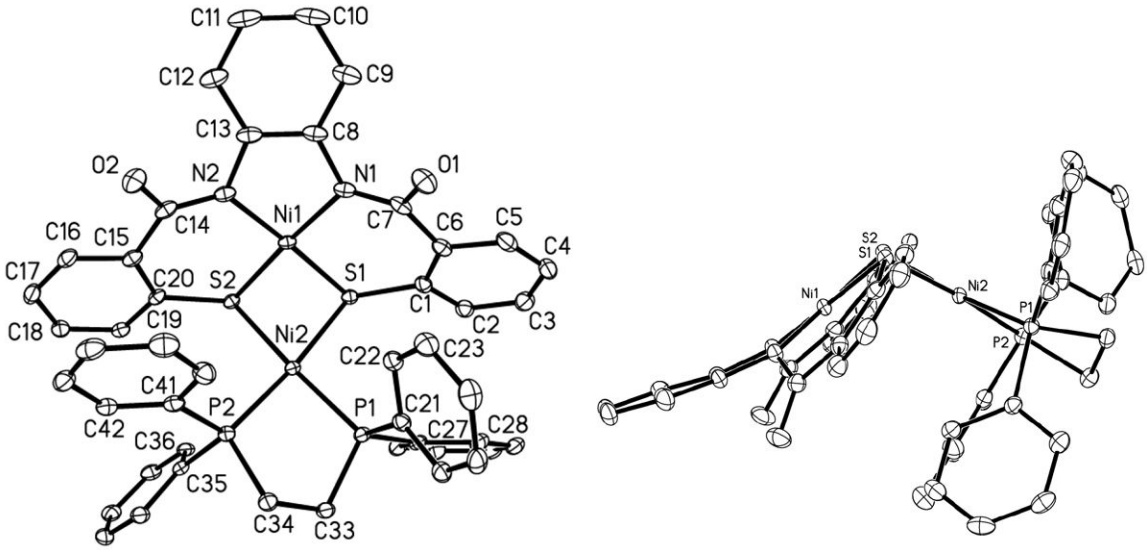

Figure 9.

ORTEP diagram of [Ni(dppe)Ni(PhPepS)] (**10**) (50 % probability) with the atom-labeling scheme (left). H atoms are omitted for the sake of clarity. A different view is shown on left showing the dihedral angle between the NiN_2S_2 and NiS_2P_2 plane.

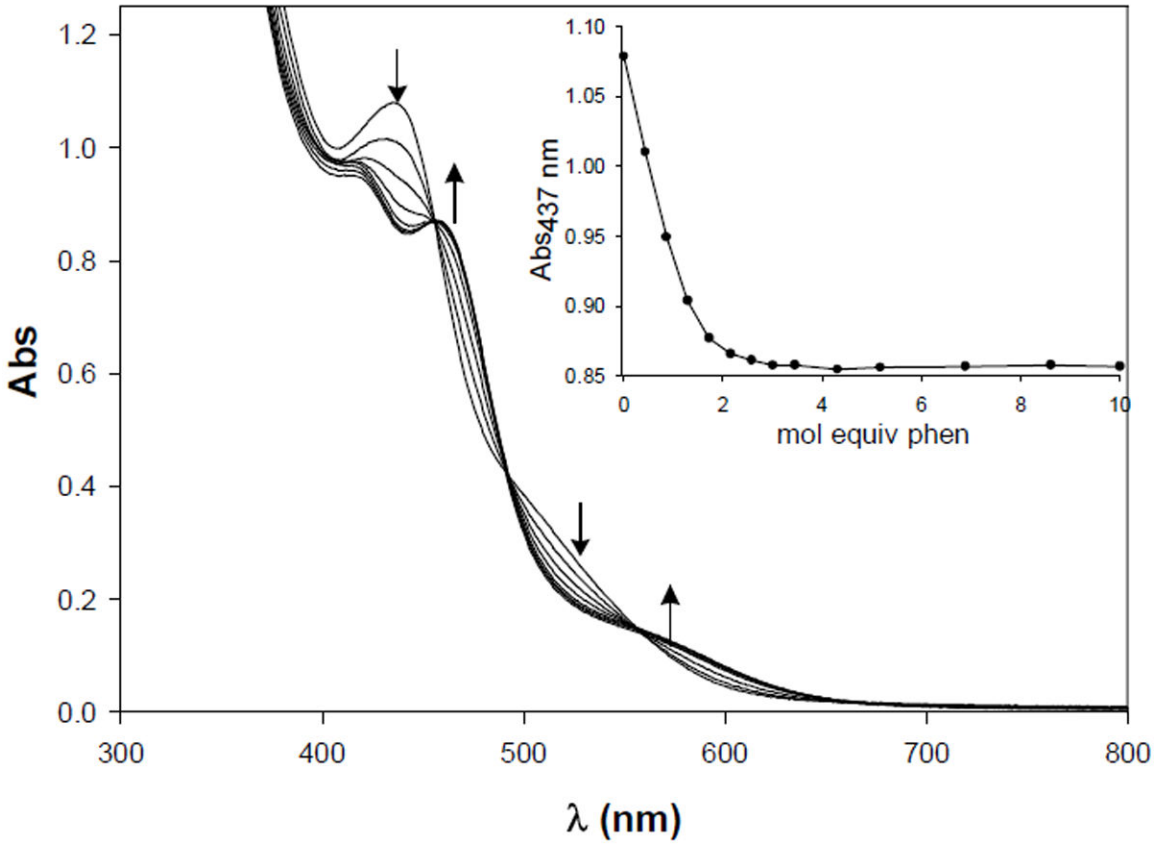

Figure 10.

Changes in the electronic absorption spectrum of $(Et_4N)_2[Ni(DMF)_2\{Ni(NpPepS)\}_2]$ (**6**, 0.087 mM) upon addition of 0.5 mol equiv aliquots of phen in DMF. Inset: change in Absorbance at 437 nm vs. mol equiv of phen.

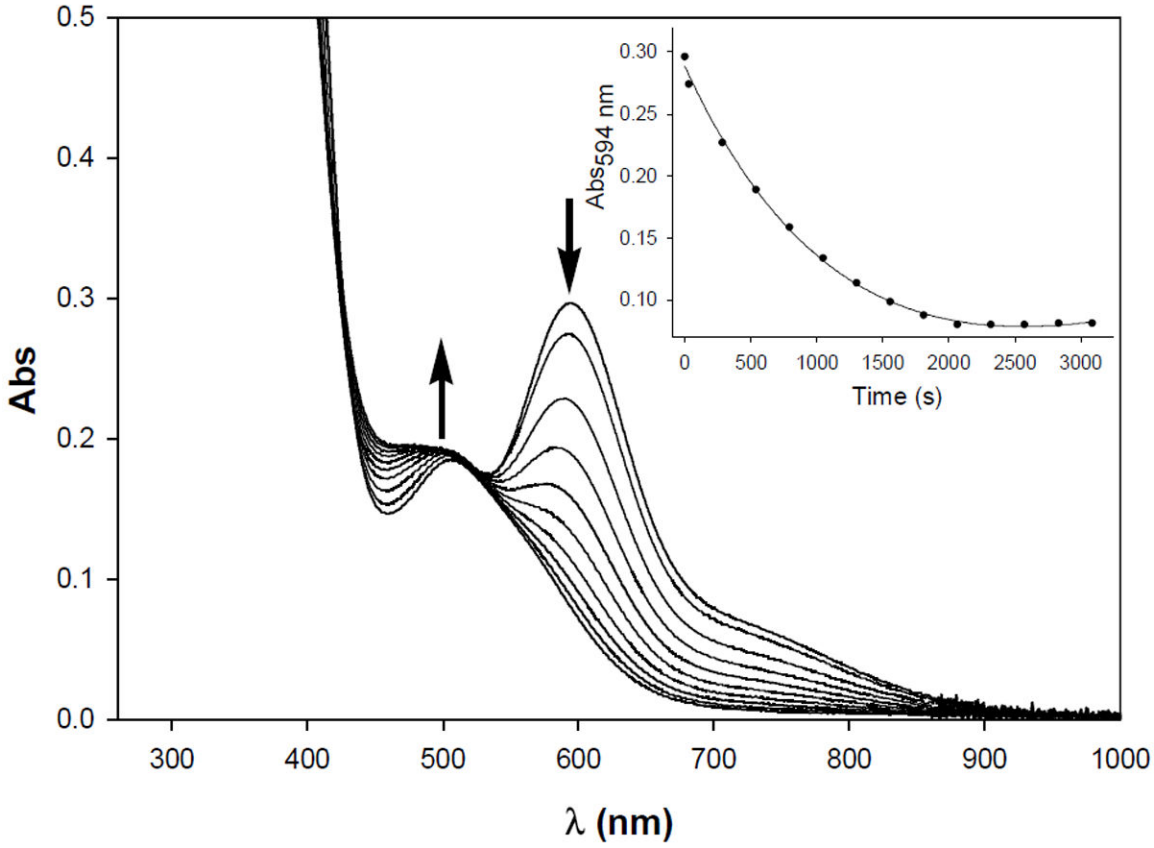

Figure 11.

Changes in the electronic absorption spectrum of [Ni(dppe)Ni(PhPepS)] (**10**, 0.0974 mM) upon mixing with excess 1,10-phenanthroline (25 mol equiv) in CH_2Cl_2 at 298 K. Inset: change in Absorbance at 594 nm vs. Time (s).

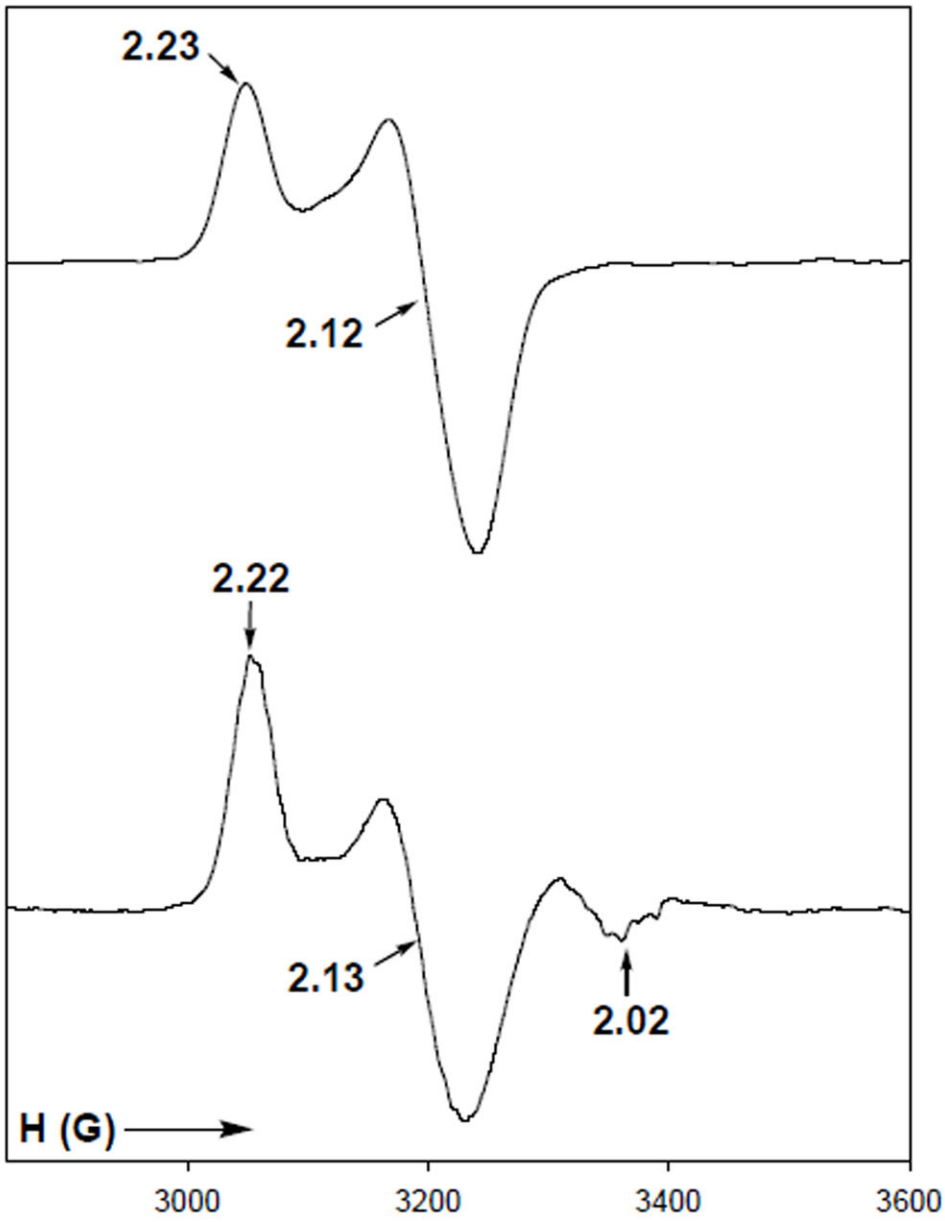

Figure 12.

X-band EPR spectra of [Ni^{I}(terpy)Ni^{II}(NpPepS)]$^{-}$ (**9_{red}**, Top) and [Ni^{I}(terpy)(CO)Ni^{II}(NpPepS)]$^{-}$ (**9_{red}-CO**, Bottom) in DMF glass at 100 K. Selected *g* values are indicated. Spectrometer settings: microwave frequency, 9.50 GHz; microwave power, 20 mW; modulation frequency, 100 kHz; modulation amplitude, 5 G.

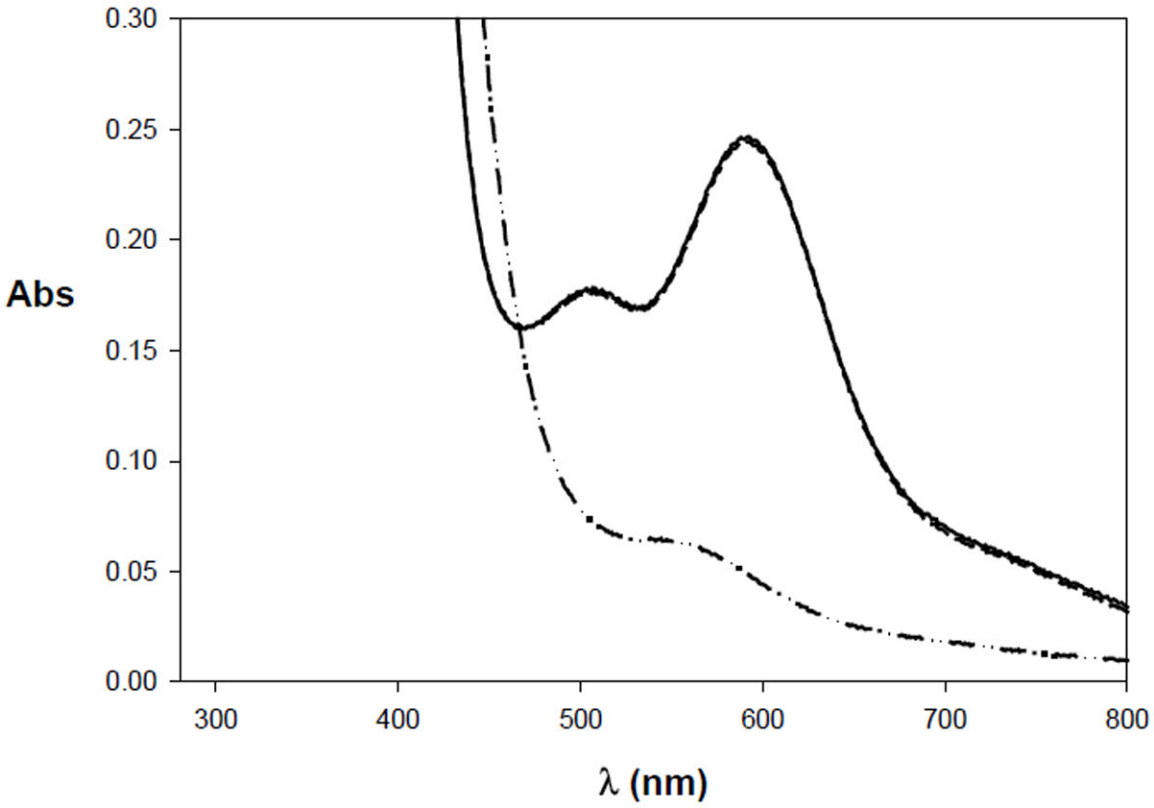

Figure 13.

Electronic absorption spectrum of [[Ni^{II}(dppe)Ni^{II}(PhPepS)] (**10**) (solid line) and its reduced species [Ni^{I}(dppe)Ni^{II}(PhPepS)]$^{-}$ (**10_{red}**) (dash-dotted line). Reoxidation of **10_{red}** to **10** upon exposure to air in CH_2Cl_2 is shown by the dashed line. The complex **10** was reduced with cobaltocene.

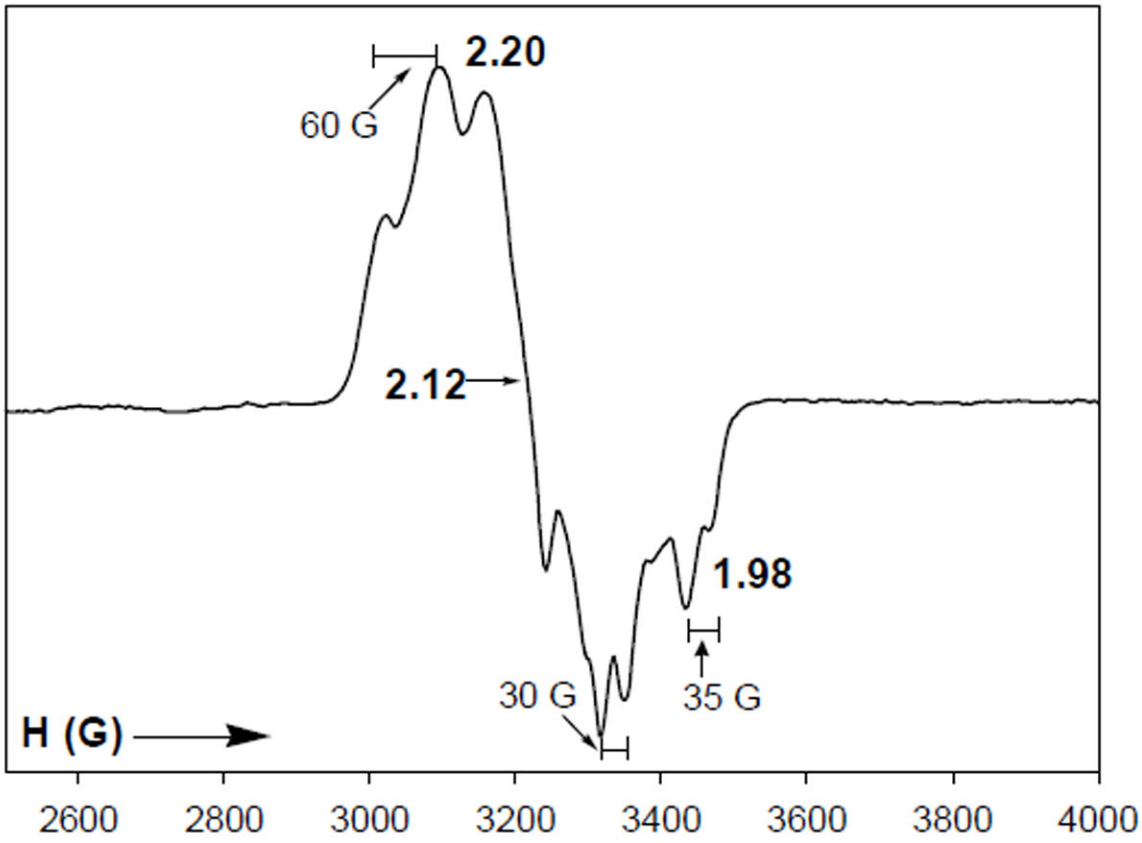

Figure 14.

X-band EPR spectrum of $[Ni^{I}(dppe)(CO)Ni^{II}(PhPepS)]^{-}$ (**10_{red}-CO**) in DMF glass at 100 K. Selected *g* and *a* values are indicated. Spectrometer settings: microwave frequency, 9.50 GHz; microwave power, 20 mW; modulation frequency, 100 kHz; modulation amplitude, 5 G.